Mineralogical Magazine (2019), **83**, 435–451
doi:10.1180/mgm.2019.10

CAMBRIDGE UNIVERSITY PRESS

Article

Substitution mechanisms in In-, Au-, and Cu-bearing sphalerites studied by X-ray absorption spectroscopy of synthetic compounds and natural minerals

Olga N. Filimonova[1], Alexander L. Trigub[1,2], Dmitriy E. Tonkacheev[1], Max S. Nickolsky[1,8], Kristina O. Kvashnina[3,7], Dmitriy A. Chareev[4,5,6], Ilya V. Chaplygin[1], Elena V. Kovalchuk[1], Sara Lafuerza[3] and Boris R. Tagirov[1]*

[1]Institute of Geology of Ore Deposits (IGEM RAS), 35, Staromonetnyi per., 119017 Moscow, Russia; [2]National Research Centre 'Kurchatov Institute', 1 Akademika Kurchatova pl., 123182 Moscow, Russia; [3]ESRF – EFiguropean Synchrotron Radiation Facility, 71, avenue des Martyrs, CS40220, 38043 Grenoble Cedex 9, France; [4]Institute of Experimental Mineralogy (IEM RAS), 142432 Chernogolovka, Moscow Region, Russia; [5]Institute of Physics and Technology, Ural Federal University, Mira st., 19, 620002 Ekaterinburg, Russia; [6]Institute of Geology and Petroleum Technologies, Kazan Federal University, Kremlyovskaya, 4/5, 420008, Kazan, Russia; [7]Helmholtz-Zentrum Dresden-Rossendorf (HZDR), Institute of Resource Ecology, P.O. Box 510119, 01314, Dresden, Germany; and [8]Frumkin Institute of Physical Chemistry and Electrochemistry, Russian Academy of Sciences, Leninskii pr. 31, korp. 4, Moscow, 119071 Russia

Abstract

Sphalerite is the main source of In – a 'critical' metal widely used in high-tech electronics. In this mineral the concentration of In is commonly correlated directly with Cu content. Here we use X-ray absorption spectroscopy of synthetic compounds and natural crystals in order to investigate the substitution mechanisms in sphalerites where In is present, together with the group 11 metals. All the admixtures (Au, Cu, In) are distributed homogeneously within the sphalerite matrix, but their structural and chemical states are different. In all the samples investigated In^{3+} replaces Zn in the structure of sphalerite. The In ligand distance increases by 0.12 Å and 0.09–0.10 Å for the 1st and 2nd coordination shells, respectively, in comparison with pure sphalerite. The In–S distance in the 3rd coordination shell is close to the one of pure sphalerite. Gold in synthetic sphalerites is coordinated with sulfur (N_S = 2.4–2.5, R_{Au-S} = 2.35 ± 0.01 Å). Our data suggest that at high Au concentrations (0.03–0.5 wt.%) the Au_2S clusters predominate, with a small admixture of the Au^+ solid solution with an Au–S distance of 2.5 Å. Therefore, the homogeneous character of a trace-element distribution, which is commonly observed in natural sulfides, does not confirm formation of a solid solution. In contrast to Au, the presence of Cu^+ with In exists only in the solid-solution state, where it is tetrahedrally coordinated with S atoms at a distance of 2.30 ± 0.03 Å. The distant coordination shells of Cu are disordered. These results demonstrate that the group 11 metals (Cu, Ag and Au) can exist in sphalerite in the metastable solid-solution state. The solid solution forms at high temperature via the charge compensation scheme $2Zn^{2+} \leftrightarrow Me^{+} + Me^{3+}$. The final state of the trace elements at ambient temperature is governed by the difference in ionic radii with the main component (Zn), and concentration of admixtures.

Keywords: Indium, gold, copper, cadmium, trace elements, sphalerite, synthetic minerals, X-ray absorption spectroscopy, EXAFS

(Received 17 August 2018; accepted 18 January 2019; Accepted Manuscript online: 4 March 2019; Associate Editor: G. Diego Gatta)

Introduction

Indium is a critical metal that is of high demand in high-tech industries. It is used worldwide for the production of flat-panel displays and touchscreens, in the manufacture of photovoltaic cells and fibre-optics, and other important industrial applications (Mercer, 2015). The global primary production of In almost doubled during 2001–2011 and reached 759 t in 2015 and 655 t in 2016 (Tolchin, 2017). The concentration of In in natural environments is low and In minerals are rare. Instead, it is concentrated in the principal sulfide ore-forming minerals with sphalerite being the most important (Schwarz-Schampera, 2014). The In content in sphalerite is usually between 0.1 and 100 ppm, but can reach several wt.% in minerals formed at temperatures between 400 and 725°C in volcanic fumaroles (Chaplygin *et al.*, 2007), or in association with roquesite ($CuInS_2$) in hydrothermal ores subjected to recrystallisation during metamorphic events (Burke and Kieft, 1980). Commonly the concentration of In directly correlates with the concentration of Cu, which implies the formation of a solid solution by the coupled substitution mechanism $2Zn^{2+} \leftrightarrow Cu^{+} + In^{3+}$ (e.g. Johan, 1988; Chaplygin *et al.*, 2007; Cook *et al.*, 2009).

Indium is obtained as a by-product of mining and beneficiation of Zn ore. The most significant sources of In are sulfidic Zn and Zn–Cu ores of volcanogenic base-metal sulfide (VMS) deposits (Mercer, 2015; Schwarz-Schampera, 2014). Many of these deposits and their modern analogues – ores of submarine hydrothermal fields – contain Au in large amounts (Bortnikov *et al.*, 2003; Melekestseva *et al.*, 2017). Some VMS deposits belong to world-class gold mines with more than 100 t Au (e.g. Mercier-Langevin *et al.*, 2011; Vikentyev *et al.*, 2004, 2015). Determination of Au concentration in submarine polymetallic

***Author for correspondence:** Boris R. Tagirov, Email: boris1t@yandex.ru
Cite this article: Filimonova O.N., Trigub A.L., Tonkacheev D.E., Nickolsky M.S., Kvashnina K.O., Chareev D.A., Chaplygin I.V., Kovalchuk E.V., Lafuerza S. and Tagirov B.R. (2019) Substitution mechanisms in In-, Au-, and Cu-bearing sphalerites studied by X-ray absorption spectroscopy of synthetic compounds and natural minerals. *Mineralogical Magazine* **83**, 435–451. https://doi.org/10.1180/mgm.2019.10

sulfide ores from the Valu Fa Ridge (the Lau basin, South-West Pacific) has showed that the Au-bearing assemblages are dominated by Fe-poor sphalerite (Herzig *et al.*, 1993). The content of gold in sphalerites of Ural VMS deposits varies between a few ppm and a few tens of ppm (Vikentyev, 2015). Thus, In, Cu and Au can be extracted as main (Cu) or by-product (In, Au) commodities from sphalerite-bearing sulfide ores.

Investigations of spectroscopic properties of pure and doped ZnS is mostly driven by the strive to produce technical applications of these materials (c.f., Yen and Weber, 2004; Schnorr, 2015). Recently, doped semiconductor nanocrystals (quantum dots) have drawn significant attention due to their unique electronic and optical properties (Norris *et al.*, 2008). Apple and Williams (1959) and Koelmans (1960) synthesised and studied ZnS phosphors activated with In and group 11 metals (Ag, Cu). It was suggested that the formation of In-bearing hexagonal ZnS (wurtzite) requires the formation of a vacancy in the cationic sublattice: $3Zn^{2+} \leftrightarrow 2In^{3+} + \square$ (Koelmans, 1960). Incorporation of In resulted in a substantial increase of the ZnS lattice constants which confirmed the solid-solution formation. However, slow cooling from the synthesis temperature, or reheating to $T > 600$°C, removed fluorescence of the material. The lattice spacings of annealed samples were found to be equal to those of pure ZnS. An association between the charged In^{3+} ion and the vacancy in the cationic sublattice was suggested to cause the emission drop and the lattice constants decrease. Therefore, the suggested charge compensation scheme seems to be valid only when In-bearing ZnS is rapidly quenched from the formation (synthesis) temperature, whereas slow cooling or reheating (metamorphism) of natural ores results in redistribution of impurities. Note that the coupled Cu–In substitution is not a required condition for the formation of In-bearing sphalerites because both Cu- and In-bearing ZnS materials have been synthesised separately for technical applications.

The phase relations and cationic substitution mechanisms in the system ZnS–$CuInS_2$ were studied by X-ray and neutron diffraction in Schorr and Wagner (2005), Schorr *et al.* (2006), and references therein. It was determined that Cu and In form a partial binary solid solution $Zn_{2x}(CuIn)_{1-x}S_2$ with a miscibility gap in the region $0.1 \leq x \leq 0.4$ (in other words, the miscibility gap extends from $Zn_{0.2}(CuIn)_{0.9}S_2$ to $Zn_{0.8}(CuIn)_{0.6}S_2$). In the region indicated the Zn-rich cubic phase coexists with tetragonal Cu and an In-rich phase, which occurs in the form of tetragonal domains ($x \approx 0.1$) in the cubic matrix ($x \approx 0.4$). These data indicate that natural Cu–In-bearing sphalerite represents a solid solution which crystallises in the cubic sphalerite-type structure, and confirm the $2Zn \leftrightarrow (Cu + In)$ substitution scheme.

The atomic and electronic structures of synthetic sphalerites doped with Mn, Fe, Co and Ni were studied using X-ray absorption spectroscopy (XAS) by Ławniczak-Jabłońska and Gołacki (1994), Ławniczak-Jabłońska *et al.* (1995, 1996) and Iwanowski *et al.* (1996, 1997, 1998). The authors showed that these impurities are incorporated into the cationic position of the sphalerite lattice, evaluated the metal-to-ligand distances in the doped sulfide, and calculated covalent radii of the dopants in a tetrahedral environment. Pattrick *et al.* (1998) studied the local atomic structure of sphalerites doped with Mn, Cu/In and Cd. The concentration of $CuInS_2$ in synthesised sphalerites was 8–20 at.%. It was found that these metals are incorporated into the sphalerite cationic sublattice, and the S tetrahedra around Cu are compressed, while around In and other dopants they are expanded. In addition, the authors detected that In/In and Cu/In clustering occurs at these high concentrations of dopants (note that much lower admixture concentrations are pertinent for natural sphalerites). Similar results on the interatomic distances in the first coordination shells of In and Cu were reported in Fieber-Erdmann *et al.* (1999) where several samples of $Zn_{2x}(CuIn)_{1-x}S_2$ (x = 0.04–1) thin films deposited on soda-lime glass substrates were studied by means of extended X-ray absorption fine structure (EXAFS) spectroscopy.

The local atomic structure of ZnS phosphors doped with Cu and Mn was studied by EXAFS spectroscopy by Warkentin *et al.* (2007). An important result of this study is that Mn substitutes for Zn in the cubic ZnS lattice, whereas Cu is present in the ZnS matrix mainly in the form of CuS clusters with only a small fraction of Cu substituting for Zn. The EXAFS data analysis suggests that the CuS clusters are integrated into the ZnS matrix and "do not have a completely random orientation, i.e. there is no any amorphous layer between the CuS-like nanocrystallites and the host crystal" (Warkentin *et al.*, 2007). The formation of CuS nanosized precipitates in the ZnS matrix was confirmed by an EXAFS study of Cu-doped ZnS nanoclusters reported in Corrado *et al.* (2009). The XAS studies of trace elements (Ge, Cu and Mn) in natural sphalerites are limited to the X-ray absorption near edge structure (XANES) spectra because of small grain sizes, their zoned character, and low concentration of the admixtures (Cook *et al.*, 2012, 2015; Belissont *et al.*, 2016; Bonnet *et al.*, 2017).

The objective of the present study is to determine the state (local atomic environment, position in the host mineral structure, valence state) of In and the group 11 metals (Cu and Au) in sphalerite, including the possibility of In–In, Au–Au, Au–In and Cu–In clustering in Au–In- and Cu–In-bearing sphalerites. In our recent study of the synthetic analogues of minerals (Tonkacheev *et al.*, 2015) we found that, similar to Cu and In, the concentrations of Au and In in sphalerite are directly correlated. In order to determine the properties of In and Au in sphalerite, we introduced these impurities into synthetic pure and Fe-bearing sphalerites and studied the synthesised crystals using XAS. In addition, the other elements which are usually present in natural sphalerites (Mn, Cd and Se) were added to one sample of synthetic Au–In-bearing sphalerite in order to verify if they can affect the state of Au and In. A sample of natural Cu–In-bearing sphalerite (+Cd, Fe and Mn), formed at 725°C in active fumaroles at the Kudriavy volcano (Iturup Island, Russia), was used to study the state of Cu and In using XAS. The use of synthetic Au–In-bearing crystals with elevated concentrations of admixtures enabled us to acquire not only XANES spectra, but to obtain good quality EXAFS results and, as a result, properly characterise the local atomic environment of In and Au. An important advantage of the use of Au, the heaviest group 11 stable atom, is that in the case of Au–In clustering the contribution of the Au atom to the In *K*-edge EXAFS spectra can be recognised by spectra analysis in contrast to the comparably light atom of Cu, which cannot be discriminated from Zn or Fe. The High Energy Resolution Fluorescence Detection mode was employed (HERFD-XAS, Glatzel and Bergman, 2005) to measure Au-bearing samples. The measurement of HERFD-XANES spectra allowed observation of important spectral features not manifested in Total Fluorescence Yield (TFY) detection (Tagirov *et al.*, 2016; Trigub *et al.*, 2017).

Results of our experiments show that In in sphalerite exists in the solid-solution state. The state of Cu and Au are different: Cu is in the solid solution, whereas Au, despite homogeneous

https://doi.org/10.1180/mgm.2019.10 Published online by Cambridge University Press

distribution and possibility of charge compensation substitution, mostly forms Au_2S clusters with only small fractions of the Au solid solution. The reasons for the contrasting behaviour of the cations are discussed below and applied to interpretation of the state of trace elements in natural Zn ores.

Methods

Methods of synthesis

The crystal growth experiments were performed as described in Chareev *et al.* (2017) using (1) the gas transport method, and (2) the salt flux technique (KCl/NaCl eutectic mixture, Chareev, 2016, Chareev *et al.*, 2016). In the gas transport method NH_4Cl was used as a transport agent. The initial phases (~0.5 g of ZnS – commercial ultrapure reagent (wurtzite), with FeS up to 10 wt.%), and, if necessary, several milligrams of MnS, CdS, ZnSe and In_2S_3 were powdered and loaded into a silica glass ampoule (8 mm ID, 11 mm OD, ~110 mm long) together with Au wire and either ~ 5 mg of transport agent or salt flux which filled the rest of the ampoule volume. The loaded ampoules were evacuated, sealed, and placed into a horizontal tube furnace which was then heated to the synthesis temperature over a period of 2–3 h, and then kept at this temperature for 20–30 days. The temperature gradient in the furnace was 50–100°C, and the measured temperature at the hot end of the ampoules was 850°C. At the end of the experiment the ampoules were quenched in cold water. Sphalerite crystals were deposited at the cold end.

Gold sulfide $Au_2S_{(cr)}$ was synthesised by sulfidising an aqueous Au cyanide solution at an ambient temperature as described in Tagirov *et al.* (2006).

Analytical methods

The morphology of the synthesised minerals was studied using scanning electron microscopy (SEM), phase compositions were obtained using X-ray diffraction (XRD), chemical composition was determined by means of electron probe micro-analysis (EPMA) and laser ablation inductively coupled mass spectrometry (LA-ICP-MS). The EPMA and LA-ICP-MS analyses were performed on polished sphalerite grains mounted in epoxy. The SEM studies were undertaken using a JSM-5610LV electron microscope equipped with an INCA-450 energy-dispersive spectrometer. EPMA were performed using JEOL JXA-8200 WD/ED combined electron probe microanalyser equipped with five wavelength-dispersive X-ray spectrometers. For Zn, Cu, Fe, Cd, In and S the operating conditions were: 20 kV accelerating voltage, 20 nA beam current and counting time of 10 s. The lines and crystals used were: Zn, Cu and Fe: *K*α (LiF crystal); Cd: *L*α (PET); In: Lα (PETH); and S: *K*α (PETH). Calibration reference materials were: chalcopyrite $CuFeS_2$ (for Fe), pure sphalerite ZnS and greenockite CdS (for Zn, S and Cd), and InSb (for In). The concentration of Au in synthetic sphalerite samples was determined using the LiF crystal accounting for the background dip immediately adjacent to the Au*L*α line from the short-wavelength side (Self *et al.* 1990). The detection limit (2σ) for Au was 0.01 wt.% at 100 nA beam current and a counting time of 100 s. In the natural sample the PETH crystal and *M*α line were used. The detection limit (2σ) for Au was 0.003 wt.% at 300 nA beam current and a counting time of 200 s.

Concentrations of ^{197}Au and ^{113}In isotopes in the synthesised sphalerite crystals, and the distribution modes (homogeneous/inhomogeneous) of Au and In were determined using a New Wave 213 laser (ESi) coupled with the Thermo Scientific X Series 2 quadrupole ICP-MS. The laser pulse frequency was 10 Hz with the power of 6–8 J/cm^2 and beam size of 40–60 μm. The analysis was carried out for 30 s preceded by 20 s for the gas blank. The ablation was performed in He + 6% H_2 (0.6 L/min) atmosphere. The gas carrying ablated material to the ICP mass spectrometer was mixed with Ar (0.8 L/min). Sulfide reference material MASS-1 (Wilson *et al.*, 2002) was used as an external calibration standard for both In and Au together with in-house pyrrhotite $Fe_{0.9}S$. Isotopes ^{68}Zn or ^{33}S were used as internal standards. The detection limit for Au (2σ) was 0.1 ppm. A scan speed of 5 μm/s was used for analyses along linear pathways.

X-ray absorption spectroscopy (XAS)

X-ray absorption experiments (i.e. collection of X-ray absorption spectra in the energy range near the core-level of the specified element) were performed at the European Synchrotron Radiation Facility (ESRF) in Grenoble, France; and Kurchatov Synchrotron Radiation Source (KSRS) in Moscow, Russia. An X-ray absorption spectrum comprises XANES data (~50–80 eV from the absorption edge) that provides information about the electronic structure and coordination geometry (Mottana, 2004), and EXAFS data (~1000 eV from the absorption edge), that provides information on the radii of coordination shells and coordination numbers (Galoisy, 2004) around the absorbing atom. In our investigation X-ray absorption spectra were recorded in two modes: TFY (In, Fe, Zn and Cd) and HERFD (Au). Details on the physical principles and experimental realisation of TFY and HERFD-XAS methods are given elsewhere (see, for example, Glatzel and Bergman, 2005; Glatzel *et al.*, 2013; Kvashnina and Scheinost, 2016). The HERFD mode yields spectral features much more intense compared to the TFY (Glatzel *et al.*, 2013) which is of crucial importance for Au-bearing sulfides with predominantly covalent bonding and smooth XANES character (c.f., Tagirov *et al.*, 2016).

The Au L_3-edge spectra were collected at the high-brilliance X-ray absorption/X-ray emission spectroscopy undulator beamline ID26 (Gauthier *et al.* 1999) of the ESRF. The storage-ring operating conditions were 6.0 GeV and the ring current was varied between 150 and 200 mA. The incident energy was selected using the <111> reflection from a double Si crystal monochromator. Rejection of higher harmonics was achieved by three Pd mirrors positioned at an angle of 2.5 mrad relative to the incident beam. The incident X-ray beam had a flux of ~2×10^{13} photons s^{-1} on the sample position. The spectra were measured in HERFD mode using an X-ray emission spectrometer (Glatzel and Bergman, 2005; Kvashnina and Scheinost, 2016). The sample, the analyser crystal and the photon detector (silicon drift diode) were arranged in a vertical Rowland geometry. The Au L_3-edge HERFD-XAS spectra were obtained by recording the intensity of the Au $L\alpha_1$ emission line (9713 eV) as a function of the incident energy. The emission energy was selected using the <555> reflection of four spherically bent Ge crystal analysers (1 m curvature radius) aligned at a Bragg angle of 78°. A combined (incident convoluted with emitted) energy resolution of 1.5 eV was determined as the full width at half maximum of the elastic peak. The intensity was normalised to the incident flux. Energy calibration was carried out using the L_3-edge

https://doi.org/10.1180/mgm.2019.10 Published online by Cambridge University Press

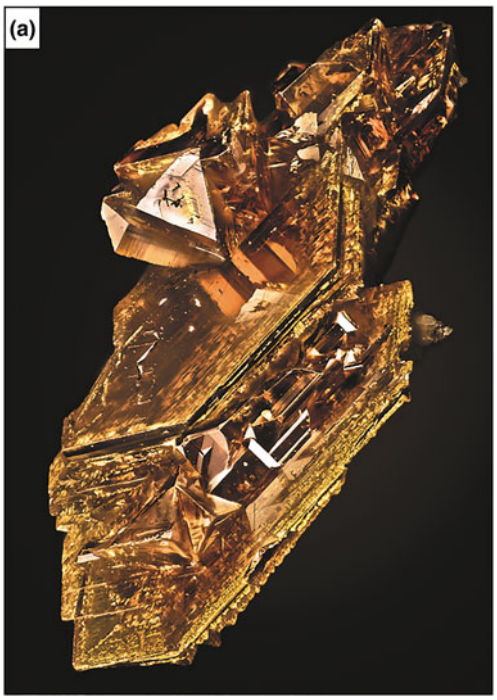

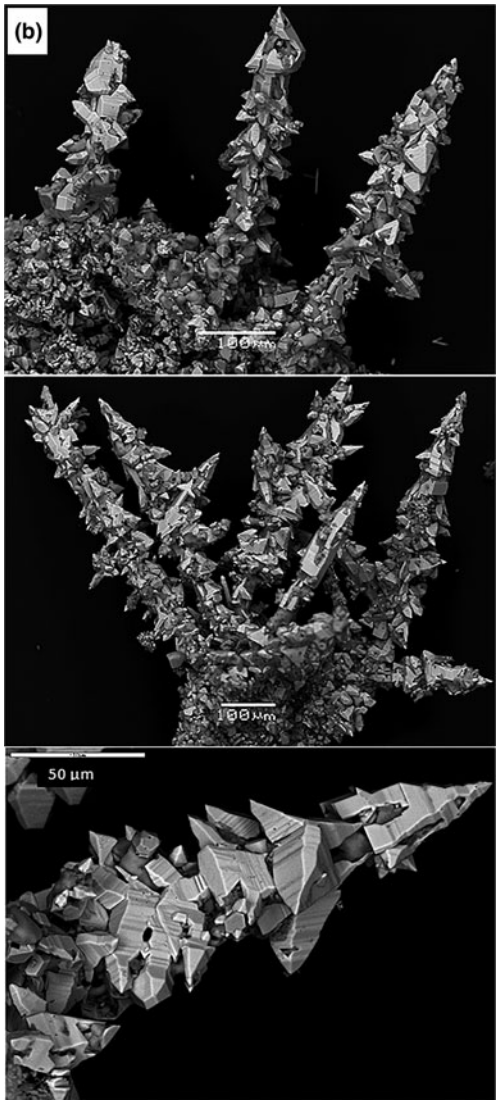

Fig. 1. (*a*) Optical microscope image of an aggregate of synthetic Au–In-bearing sphalerite crystals (Sample 1661). Concentrations of admixtures: 1.9 wt.% Fe; 0.22 wt.% In; and 0.25 wt.% Au. Field of View = 0.3 mm × 0.4 mm. Photo by T. Pashko. (*b*) Back-scattered electron images of crystals of natural Cu–In-bearing sphalerite (Sample 501).

excitation energy of Au (11,919 eV) by recording the spectra of Au foil before measuring each sample.

The In and Cu *K*-edge spectra were recorded at the Rossendorf Beamline BM20 of the ESRF. The storage-ring operating conditions were 6.0 GeV and 80–100 mA. The photon energy was scanned from 27700 to 28570 eV (In) and 8600 to 9900 eV (Cu) using the Si(111) monochromator coupled to Rh-coated mirrors for the collimation and reduction of higher harmonics. Energy calibration was performed using the *K*-edge excitation energy of In (27,940 eV) and Cu (8979 eV) metal foil. The spectra of the metal foils, placed immediately after the samples between the 2nd and 3rd ionisation cameras, were recorded in transmission mode simultaneously with the spectra of the samples. The spectra of reference substances were collected in transmission mode while the spectra of sphalerite samples were recorded in TFY mode using a 13-element high-throughput Ge-detector. The total energy resolution (incident energy and core-hole lifetime broadening) has been evaluated as 8.8 eV. The detected intensity was normalised to the incident photon flux.

The Zn, Fe and Cd *K*-edge spectra were measured at the Structural Materials Science station (Chernyshov *et al.*, 2009) of the KSRS. The storage-ring operating conditions were 2.3 GeV and 80–100 mA. A Si(111) monochromator was used and the energy calibration was performed using the *K*-edge absorption energy of Zn, Fe and Cd foils. The X-ray absorption spectra of Zn in sphalerite samples were registered in transmission mode and the spectra of Fe and Cd in fluorescence mode using an avalanche photodiode (FMB OXFORD). The spectra of standards (pure synthetic minerals FeS_2 and CdS) were recorded in transmission mode.

Fig. 1. Continued

EXAFS spectra fitting

The EXAFS ($\chi_{exp}(k)$) data were analysed using the *IFEFFIT* package (Ravel and Newville, 2005). Following standard procedures for pre-edge subtraction and spline background removal, the structural parameters [interatomic distances (R_i), coordination numbers (N_i) and Debye–Waller factors (σ_i^2)] were determined via the non-linear fit of theoretical spectra to the experimental ones with the equation

$$\chi(k) = S_0^2 \sum_{i=1}^{n} \frac{N_i F_i(k)}{R_i^2 k} e^{\frac{-2R_i}{\lambda(k)}} e^{-2\sigma_i^2 k^2} \sin(2kR_i + \varphi_i(k)). \quad (1)$$

Theoretical spectra were simulated using photoelectron mean free-path length $\lambda(k)$, amplitude $F_i(k)$ and phase shift $\varphi_i(k)$ parameters calculated *ab initio* using the program *FEFF6* (Zabinsky *et al.*, 1995).

https://doi.org/10.1180/mgm.2019.10 Published online by Cambridge University Press

Density Functional Theory (DFT) calculations

The objective of these calculations was to investigate the substitution mechanisms in In- and Au-bearing sphalerites by modelling the local atomic environments of these elements with subsequent comparison of simulated and experimental XAS data, and to describe their charge states. In addition, a series of calculations was performed for Cd-bearing sphalerite. Details of quantum chemical DFT calculations are described in Tagirov *et al.* (2016) and Trigub *et al.* (2017). The software package *QUANTUM ESPRESSO* (Giannozzi *et al.*, 2009) was used for the calculations. We employed a projector-augmented wave all-electron description of the electron–ion–core interactions (Blöhl, 1992; Kresse, 1999) and the Perdew–Burke–Ernzerhof exchange-correlation functional. The self-consistent field (SCF) method with a 100 Ry kinetic energy cut-off for the plane waves, a 1500 Ry charge density cut-off, and a SCF tolerance $>10^{-9}$ was applied in the electronic structure calculations. The optimisations of the crystal structure and supercell parameters were performed using the Broyden–Fletcher–Goldfarb–Shanno algorithm (Fletcher, 1987) for atomic coordinates with convergence threshold 10^{-3} Ry/au for forces and 10^{-4} Ry for energy. The relaxation of the atomic positions and cell parameters were performed in a supercell that contained $3 \times 3 \times 3$ unit cells. The topological atomic charges were determined by means of the quantum theory of atoms in molecules (QTAIM, Bader, 1990; Bader, 1991). The local atomic charges were calculated by integrating the charge density within Bader volumes around the atoms (Otero-de-la-Roza *et al.*, 2009; Otero-de-la-Roza *et al.*, 2014).

Results and discussion

Concentration and distribution of admixtures

The morphology of the crystals of synthetic and natural sphalerites is shown in Figs 1*a* and *b*, respectively. Back-scattered electron images of synthetic and natural crystal grains mounted in polished sections are shown in Figs 2*a* and *b*, respectively. Time-resolved spectra of the LA-ICP-MS signal recorded for synthetic Au–In sphalerites is shown in Fig. 3. Compositions of crystals are listed in Table 1.

As a result of the synthesis experiments, aggregates of crystals with a grain size between 0.1 and 1 mm were obtained (Fig. 1*a*). The XRD pattern of synthesised samples corresponded to the pure sphalerite PDF#5-566. High-temperature (850°C) sphalerites contained extremely high (up to 0.5 wt.%) concentrations of In and Au. Both In and Au were found to be dispersed in the 'invisible' state by optical and electron microscopy (Fig. 2*a*). The concentrations of these admixtures in the synthesised crystals are close to each other and directly correlated (Table 1). The homogeneous character of In and Au distribution patterns is confirmed by (1) a small variation of measured concentrations (see uncertainties of measured concentrations in Table 1), and (2) the 'flat', smooth character of LA-ICP-MS time-resolved spectra which indicates the absence of micronuggets of In- and Au-bearing phases (Fig. 3). At the same time, some crystal aggregates were covered with metallic Au which was transported together with other metals and deposited at the cold end of the ampoule. Analyses by SEM revealed that these aggregates typically contained inclusions of Au inside the sphalerite grains (Fig. 2*a*). Therefore, during the preparation of samples for the XAS experiment, only grains where the surface was free of metallic Au were selected using binocular microscopy. The absence of the spectral features of metallic Au in the recorded XAS spectra demonstrated that the concentration of this form of Au in the selected samples was negligible.

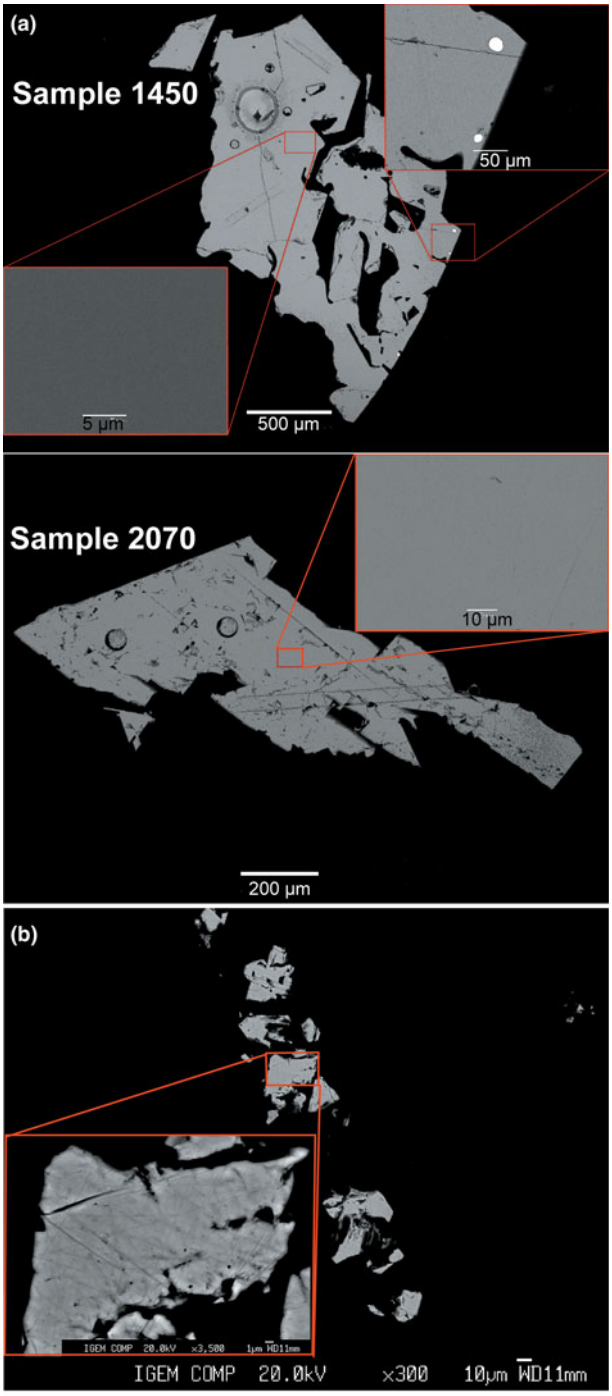

Fig. 2. Examples of back-scattered electron images of sphalerite grains. (*a*) Synthetic Au–In sphalerites. Several inclusions of metallic Au captured during precipitation of sphalerite are seen in the image of Sample 1450 (only grains free of Au inclusions were selected for the XAS experiment). (*b*) Natural Cu–In sphalerite. All the grains of sphalerite are homogeneous within the resolution of the scanning electron microscope, the composition of the samples is given in Table 1.

The natural sample (Fig 1*b*) is composed of sphalerite, probably with a minor admixture of the hexagonal phase – wurtzite (results of XRD analysis are shown in fig. 5 in Chaplygin *et al.*,

https://doi.org/10.1180/mgm.2019.10 Published online by Cambridge University Press

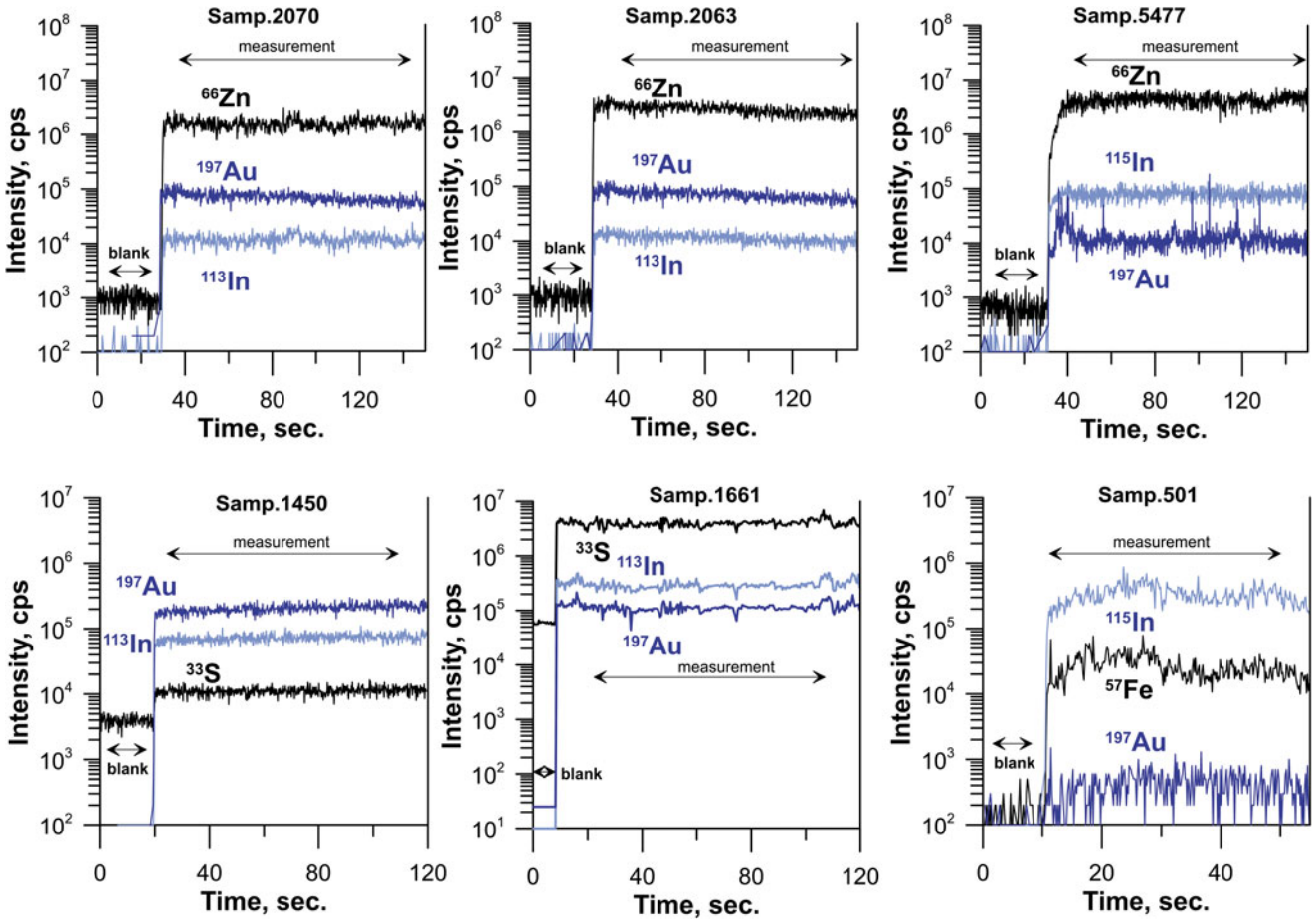

Fig. 3. Laser ablation-ICP-MS time-resolved spectra of line analysis across sphalerite grains. The compositions of samples are given in Table 1.

2007). The distribution of elements in the sphalerite grains is homogeneous (Fig. 2*b*). Apart from admixtures of In, Cu and Mn (<1 wt.% of each element), the sample contains Cd (7 wt.%) and Fe (3 wt.%) (Table 1). Note also that μm-sized Au crystals were commonly observed on the surface of grains of sphalerite and wurtzite–greenockite sampled at the Kudriavy volcano (see fig. 3c in Chaplygin *et al.*, 2007). The concentration of 'invisible' Au in the natural sphalerite sample was 7 ppm.

XANES spectroscopy

The In, Cu, Cd *K*-edge XANES and Au L_3-edge HERFD-XANES spectra of sphalerite samples are compared to the reference substances in Fig. 4. Energy positions of the edge jump and the first intense feature known as the 'white line' are listed in Table 2. The Zn and Fe *K*-edge spectra are shown in Supplementary Fig. S1. To facilitate discussion of XAS results, Fig. 5 shows the crystal structure of sphalerite with an indication of the coordination polyhedra around a cation.

Iron and zinc K-edges

Admixtures of In, Au and Cu affect neither coordination geometry of Zn/Fe, nor the Fe oxidation state (Fig. S1, left and right panels). We note, however, that XANES spectroscopy is not sensitive to minor changes of the oxidation state of the Fe admixture, which can be determined unambiguously by additional experiments with Mössbauer spectroscopy.

Indium K-edge

The edge jump and white line positions of In *K*-edge spectra are identical, independent to the concentration of In, Fe and Au in all synthetic Au–In-bearing sphalerites. This means that the concentration of Fe, Au and In itself, has a negligible effect on the local atomic environment and the valence state of In. At the same time, the edge jump and white line positions are different from those of the In_2O_3 and In_2S_3: they are shifted by 1 eV to lower energies in comparison with In_2O_3, and, on the contrary, by ~0.4 eV to higher energies compared to In_2S_3 (Table 2). This small shift is close to the uncertainty of the excitation energy, but was observed for all the sphalerite samples. Accordingly, the chemical state of In in sphalerite is different from the oxide and sulfide forms. In contrast to In_2O_3 and In_2S_3, the spectra of In-bearing sphalerites and $CuInS_2$ look similar, which suggests the similarity of the nearest-to-In atomic geometry of sphalerite and In-chalcopyrite (roquesite).

The edge jump position of Cu–In-bearing sphalerite (Sample 501) is similar to the Au–In-bearing samples, but the white line position is located at a slightly higher energy ($\Delta E = 0.5$ eV). The white line intensity is also different: it is lower than that of Au–In sphalerites which results in smoother character of the spectra. These differences are most probably due to the difference in composition of the natural sphalerite sample, which contains a high concentration of Cu (3 wt.%, Table 1) that can affect the electronic structure of the material and modify the shape of XANES spectra.

https://doi.org/10.1180/mgm.2019.10 Published online by Cambridge University Press

Table 1. Compositions of synthetic and natural sphalerites used in XAS experiments. Concentrations are given in wt.% (± 2σ).

Sample #	EPMA Zn	In	Fe	S	Au	Cd	Mn	Se	Cu	Total	Empirical formula	LA-ICP-MS Au
2070[1]	54.97	0.55	9.89	33.16	0.57	n/d	n/d	n/d		99.14	$(Zn_{0.94},Fe_{0.05})S_{1.01}$	0.560
	(1.59)	(0.01)	(0.03)	(0.28)	(0.01)					(1.74)		(0.015)
2063[1]	63.89	0.34	1.71	33.06	0.29	n/d	n/d	n/d		99.29	$(Zn_{0.96},Fe_{0.03})S_{1.01}$	0.310
	(1.00)	(0.02)	(0.07)	(0.57)	(0.03)					(1.69)		(0.004)
5477[1]	65.84	0.09	n/d	33.69	0.03	n/d	n/d	n/d		99.65	$Zn_{0.98}S_{1.02}$	0.035
	(1.26)	(0.02)		(0.69)	(0.02)					(1.99)		(0.003)
1440[2]	64.74	n/d	1.49	33.81	n/d	n/d	n/d	n/d		100.04	$(Zn_{0.95},Fe_{0.03})S$	0.020
	(1.06)		(0.02)	(0.59)						(1.3)		(0.003)
1450[2]	63.95	0.29	1.62	33.73	0.30	0.48	0.24	0.13		100.74	$(Zn_{0.95},Fe_{0.03})S$	0.29
	(0.51)	(0.02)	(0.13)	(0.32)	(0.05)	(0.11)	(0.05)	(0.07)		(0.59)		(0.05)
1661[1]	65.24	0.22	1.89	33.76	0.25	n/d	n/d	n/d		101.36	$(Zn_{0.96},Fe_{0.03})S_{1.01}$	0.21
	(0.31)	(0.03)	(0.06)	(0.53)	(0.05)					(0.55)		(0.05)
501[3]	56.32	0.20	1.75	31.73	n/d	7.52	0.14	n/d	0.12	97.78	$(Zn_{0.89},Fe_{0.03},Cd_{0.07})S$	n/d
	(53.06–57.67)	(0.06–0.35)	(0.90–4.95)	(31.39–32.01)		(6.85–8.12)	(0.09–0.17)		(0.02–0.19)	(97.11–98.87)		
501[4]	54.49	0.57	3.05	31.89	n/d	6.74	0.12	n/d	0.30	97.17	$(Zn_{0.85},Fe_{0.06},Cd_{0.06},In_{0.01})S_{1.02}$	7(2) ppm
	(2.35)	(0.30)	(1.73)	(0.38)		(0.51)	(0.03)		(0.16)	(0.69)		

[1] Salt flux synthesis method; [2] gas transport synthesis method; [3] data of Chaplygin *et al.* (2007), the range of measured concentrations is given in parentheses; [4] determined in the present study; n/d – not determined.

We can interpret the observed edge jump energy position in the sphalerites by assuming that the oxidation state of In is intermediate between In_2O_3 and In_2S_3, which means that the formal oxidation state of In in sphalerite is +3. The slightly higher energy of the edge jump position in In-bearing sphalerite in comparison with In_2S_3 can be ascribed to stronger In–S interaction in the state of the solid solution, which results in a more effective negative charge transfer from In to S similar to $CuInS_2$. The latter would result in a shorter In–S distance in In-bearing sphalerite and $CuInS_2$ compared to In_2S_3. An additional argument in favour of the compression of the 1st coordination shell is that the minimum of the XANES spectra, which separates white line and the 2nd spectral feature, is located at much higher energy of ~27,980 eV for In-bearing sphalerite than for In_2S_3 (~27,972 eV).

Gold L_3-edge

The Au L_3-edge HERFD-XANES spectra of sphalerites differ from the spectra of Au and Au_2S. The edge jump and white line positions are shifted to higher energies compared to the Au_2S spectra. The position of the second spectral feature also exhibits a large positive shift by ~3 eV. The low white line intensity in comparison with Au^{3+} state (e.g. Tagirov *et al.*, 2016) suggests that the formal oxidation state of Au is +1. The shape of the white line feature of sphalerite spectra, unlike Au_2S, is highly asymmetric which can be explained by the presence of several different geometries of the local atomic environment of Au. At the same time, the shape and positions of the spectral features are identical for In-rich and In-free sphalerites, which suggests the absence of In/Au clustering. This important conclusion was tested via EXAFS spectra analysis.

Copper K-edge

There are some small but notable differences of the spectrum of Cu–In-bearing sphalerite from the spectrum of $CuInS_2$, which are clearly distinguishable in the enlarged portion of Fig. 4*d*. The edge jump of natural sphalerite (Sample 501) is slightly (by 0.5 eV) shifted towards lower energies (Table 2). At the same time, the second spectral feature with the maximum at ~8997 eV is located at higher energy than the second feature of $CuInS_2$. In general, the shapes of XANES spectra of natural Cu–In-bearing sphalerite and $CuInS_2$ are not identical, which implies that some differences exist between the states of Cu in these phases.

The differences between the spectra of sphalerite, $CuInS_2$, and the spectrum of chalcopyrite $CuFeS_2$ are much more pronounced. The pre-edge feature, which is present in the spectrum of $CuFeS_2$, is absent in the spectra of $CuInS_2$ and natural sphalerite. The formal electronic structure of Cu is [Ar] $3d^{10}$ for Cu^{1+}, and [Ar] $3d^9$ for Cu^{2+}. Therefore, the spectral features of the Cu *K*-edge XANES correspond to dipole-allowed excitations to the empty 4*p* level for Cu^{1+} and, in addition, the pre-edge structure is most likely to correspond to the transitions from 1*s* to hybridised 3*d*-4*p* states. The same pre-edge feature is observed in the XANES Cu *K*-edge spectrum of covellite where the formal oxidation state of Cu is close to +1.3 (Tagirov *et al.*, 2016). Increase of the Cu oxidation state in $CuFeS_2$ in comparison with $CuInS_2$ results in a positive shift of the edge jump and white line positions of $CuFeS_2$ (Table 1). Therefore, the formal oxidation state of Cu in chalcopyrite falls between +1 and +2, which is associated with the formal oxidation state between +2 and +3 for Fe. The absence of the pre-edge feature in the spectra of $CuInS_2$ and Cu–In-bearing sphalerite implies that the oxidation state of Cu is +1, which is consistent with the oxidation state +3 for In.

https://doi.org/10.1180/mgm.2019.10 Published online by Cambridge University Press

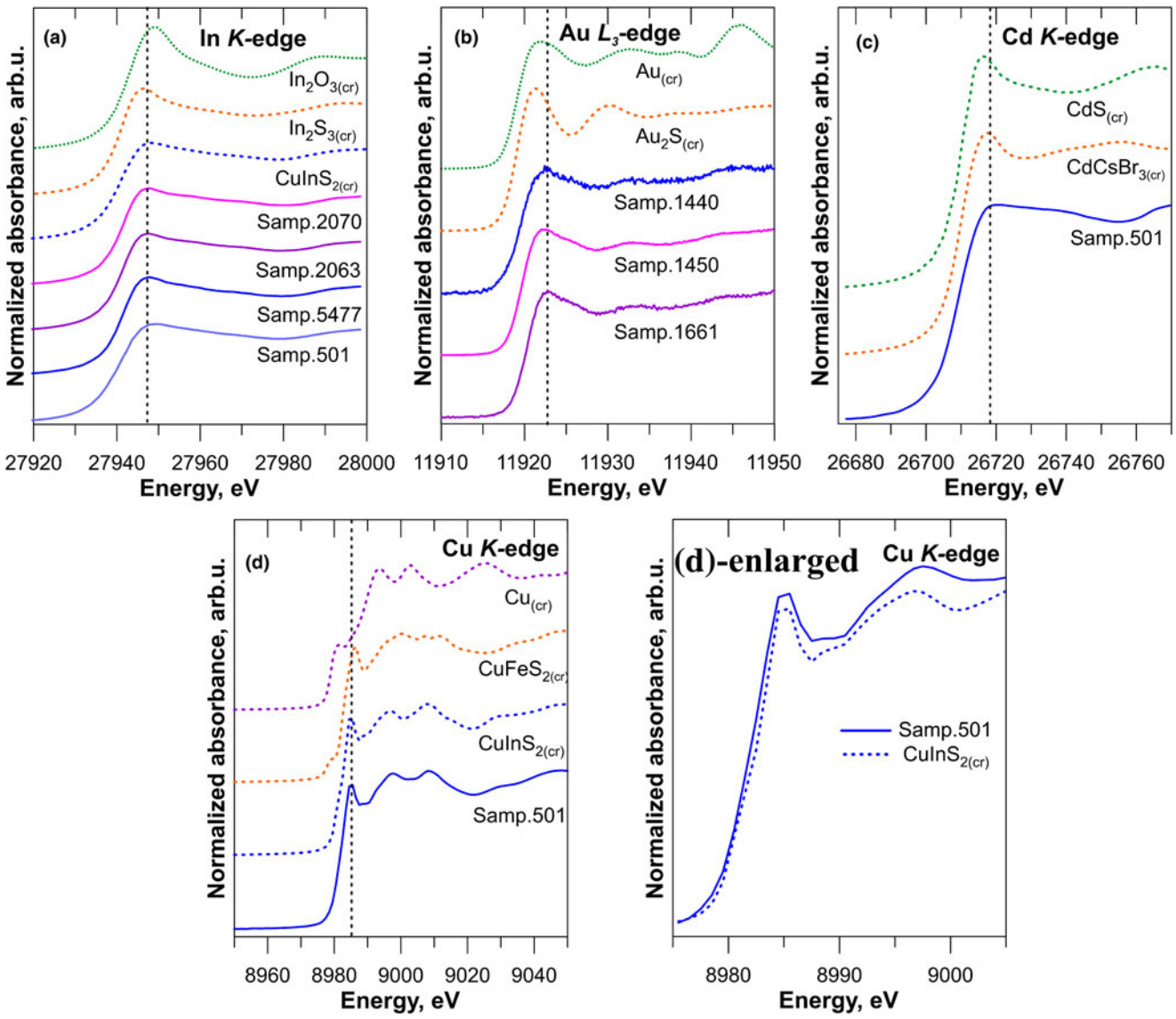

Fig. 4. (*a*) Indium *K*-edge XANES spectra of In–Au-bearing sphalerites and standards (In_2O_3 and In_2S_3); (*b*) Au L_3-edge HERFD-XANES spectra of Au ± In-bearing sphalerites and standards (Au and Au_2S); (*c*) Cd *K*-edge spectra of the natural sphalerite and standards (CdS and $CdCsBr_3$); (*d*) Cu *K*-edge XANES spectra of In–Cu-bearing natural sphalerite (Kudriavy volcano) and standards (Cu, $CuFeS_2$ and $CuInS_2$). Vertical dashed lines indicate positions of the most intense spectral features of sphalerite samples.

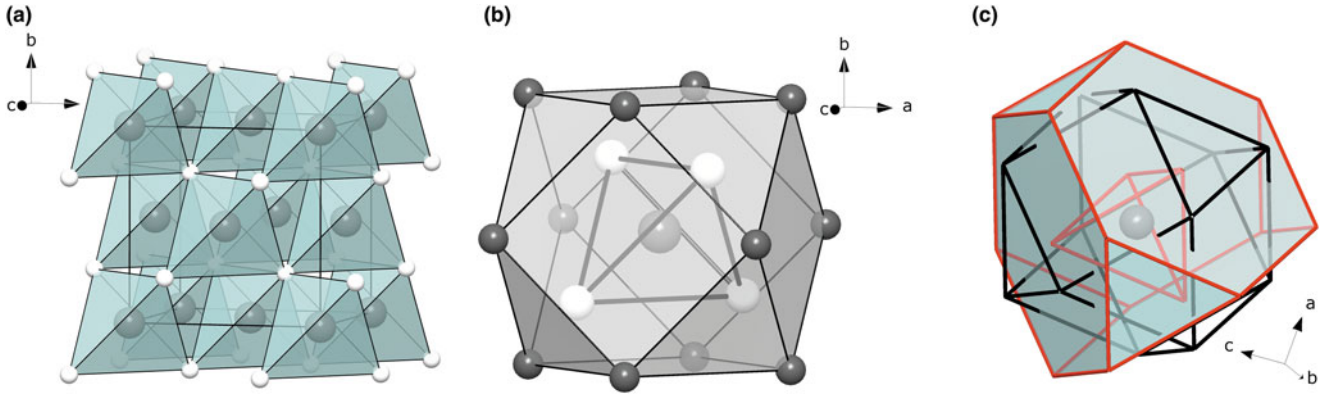

Fig. 5. (*a*) The unit cell of cubic ZnS. Large grey balls are Zn atoms, small white balls are S atoms. (*b*) First (S4 tetrahedron) and second (Zn12 cuboctahedron) coordination shells of Zn in cubic ZnS. (*c*) Three coordination shells of Zn in ZnS. Red lines correspond to S–S edges, black lines correspond to Zn–Zn edges.

https://doi.org/10.1180/mgm.2019.10 Published online by Cambridge University Press

Table 2. Positions of edge jump (e.j.) and the first intense feature (white line, WL) of In *K*-edge, Au L_3-edge, Cu *K*-edge, and Cd *K*-edge spectra of synthetic Au±In- and natural Cu–In-bearing sphalerites and standards (as determined by the *IFEFFIT* program). Uncertainty of the energy values is ±0.5 eV.

Sample, standard	Feature	Position, eV
In *K*-edge XANES		
In_2O_3	e.j.	27942.4
	WL	27948.9
In_2S_3	e.j.	27941.0
	WL	27946.0
$CuInS_2$	e.j.	27941.2
	WL	27947.9
Sample 2063	e.j.	27941.4
Fe 1.71 wt.%, In 0.34 wt.%, Au 0.31 wt.%	WL	27947.5
Sample 2070	e.j.	27941.4
Fe 9.89 wt.%, In 0.55 wt.%, Au 0.56 wt.%	WL	27947.5
Sample 5477	e.j.	27941.3
In 0.09 wt.%, Au 0.035 wt.%	WL	27947.4
Sample 501	e.j.	27941.2
Cd 7.52 wt.%, In 0.20 wt.%, Cu 0.12 wt.%	WL	27948.0
Au L_3-edge HERFD-XANES		
Au	e.j.	11919.0
	WL	11922.0
Au_2S	e.j.	11918.9
	WL	11921.2
Sample1440	e.j.	11919.2
Fe 1.49 wt.%, Au 0.02 wt.%	WL	11922.5
Sample1450	e.j.	11919.2
Fe 1.62 wt.%, In 0.29 wt.%, Au 0.29 wt.%	WL	11922.7
Sample1661	e.j.	11919.0
Fe 1.89 wt.%, In 0.22 wt.%, Au 0.21 wt.%	WL	11923.0
Cu *K*-edge XANES		
$CuFeS_2$	pre-peak	8979.3
	e.j.	8983.0
$CuInS_2$	WL	8985.9
	e.j.	8982.5
	WL	8985.0
Sample 501	e.j.	8982.0
	WL	8985.0
Cd *K*-edge XANES		
CdS	e.j.	26710.3
	WL	26716.1
$CdCsBr_3$	e.j.	26710.0
	WL	26717.2
Sample 501	e.j.	26709.0
	WL	26718.7

Cadmium K-edge

The shape of the Cd *K*-edge XANES spectra of natural sphalerite and positions of the main spectral features are different from those of the spectra of reference substances ($CdS_{(cr)}$ and $CdCsBr_3$). This means that the local atomic environment of Cd differs from $CdS_{(cr)}$ – greenockite. The formal oxidation state of Cd is +2. The 'effective' oxidation state of Cd in sphalerite, which is indicative for the electronic structure of the substance, is lower (less positive) than the oxidation state in both the references as the edge jump position is shifted to lower energies (Table 2), and the white line is of lower intensity (Fig. 4).

EXAFS spectra fitting

Results of EXAFS spectra fitting obtained using the *ARTEMIS* program of the *IFEFFIT* software package for Zn, Fe, In, Cu and Cd *K*-edges, and for the Au L_3-edge are given in Table 3 and compared with the experimental spectra in Fig. 6 (In *K*-edge), Fig. 7*a* (Au L_3-edge), Fig. 7*b* (Cu *K*-edge) and

Table 3. Zn, Fe, In, Cu, Au and Cd local atomic structure in sphalerite determined by EXAFS fitting using the *IFEFFIT* package (fit in *k*-space unless otherwise indicated, k^2 weighting). Numbers without uncertainties were fixed during the fit. Uncertainties are calculated by the *ARTEMIS* program.

Scattered atoms	*N*	*r*, Å	σ^2, Å^{-2}	E^0, eV	*R*-factor
Zn *K*-edge[1]					
Synthetic sphalerite (gas transport synthesis), *k*-range: 2.5–13					
S	4	2.34 ± 0.01	0.005 ± 0.001	4.0 ± 0.6	0.012
Zn	12	3.84 ± 0.01	0.015 ± 0.001		
S	12	4.46 ± 0.02	0.018 ± 0.003		
Sample 2070 (Fe 9.89 wt.%, In 0.55 wt.%, Au 0.57 wt.%), *k*-range: 2.5–13					
S	4.00 ± 0.44	2.34 ± 0.01	0.005 ± 0.001	4.5 ± 1.0	0.045
Zn	12	3.84 ± 0.02	0.015 ± 0.002		
S	12	4.45 ± 0.03	0.018 ± 0.005		
Sample 2063 (Fe 1.71 wt.%, In 0.34 wt.%, Au 0.29 wt.%), *k*-range: 2.5–13					
S	3.84 ± 0.44	2.34 ± 0.01	0.005 ± 0.001	5.0 ± 1.1	0.048
Zn	12	3.84 ± 0.02	0.015 ± 0.002		
S	12	4.45 ± 0.03	0.017 ± 0.005		
Sample 1450 (Fe 1.62 wt.%, In 0.29 wt.%, Au 0.30 wt.%), *k*-range: 2.5–13					
S	3.82 ± 0.45	2.34 ± 0.01	0.005 ± 0.001	5.1 ± 1.1	0.051
Zn	12	3.84 ± 0.02	0.015 ± 0.002		
S	12	4.45 ± 0.03	0.017 ± 0.005		
Sample 1661 (Fe 1.89 wt.%, In 0.22 wt.%, Au 0.25 wt.%), *k*-range: 2.5–13					
S	4.04 ± 0.45	2.34 ± 0.01	0.005 ± 0.001	5.0 ± 1.0	0.047
Zn	12	3.84 ± 0.02	0.015 ± 0.002		
S	12	4.45 ± 0.03	0.016 ± 0.005		
Fe *K*-edge[2]					
Sample 2070, *k*-range: 2.5–11					
S	3.68 ± 0.54	2.34 ± 0.01	0.003 ± 0.002	2.7 ± 1.3	0.051
Zn	12	3.84 ± 0.02	0.016 ± 0.003		
S	12	4.42 ± 0.04	0.017 ± 0.007		
Sample 2063, *k*-range: 2.5–11					
S	4.26 ± 0.82	2.34 ± 0.01	0.003 ± 0.002	1.3 ± 1.8	0.081
Zn	12	3.83 ± 0.03	0.014 ± 0.004		
S	12	4.40 ± 0.05	0.015 ± 0.008		
Sample 1450, *k*-range: 2.5–10					
S	4.84 ± 1.45	2.34 ± 0.02	0.003 ± 0.003	2.6 ± 3.3	0.097
Zn	12	3.81 ± 0.04	0.012 ± 0.004		
S	12	4.40 ± 0.15	0.027 ± 0.032		
Sample 1661, *k*-range: 2.5–11					
S	3.75 ± 0.81	2.34 ± 0.01	0.001 ± 0.002	2.5 ± 2.1	0.087
Zn	12	3.83 ± 0.03	0.013 ± 0.003		
S	12	4.43 ± 0.08	0.022 ± 0.015		
Sample 501 (Cd 7.52 wt.%, In 0.20 wt.%, 0.12 Cu wt.%), *k*-range: 2.5–11, fitting in *R*-space, *R*-Range: 1.2-4.0					
S	3.92 ± 0.56	2.29 ± 0.01	0.004 ± 0.002	1.3 ± 1.3	0.030
Zn	12	3.82 ± 0.02	0.012 ± 0.002		
S	12	4.29 ± 0.08	0.037 ± 0.020		
In *K*-edge[3]					
Sample 2063, *k*-range: 2.5–13					
S	4.22 ± 0.46	2.46 ± 0.01	0.004 ± 0.001	5.5 ± 1.2	
Zn	12	3.92 ± 0.03	0.018 ± 0.004		0.049
S	12	4.48 ± 0.04	0.016 ± 0.006		
Sample 2070, *k*-range: 2.5–13					
S	4.46 ± 0.35	2.46 ± 0.01	0.005 ± 0.001	5.0 ± 0.9	0.026
Zn	12	3.92 ± 0.02	0.018 ± 0.002		
S	12	4.48 ± 0.03	0.015 ± 0.004		
Sample 5477 (In 0.09 wt.%, Au 0.03 wt.%), *k*-range: 2.5–13					
S	4.23 ± 0.52	2.46 ± 0.01	0.005 ± 0.001	6.2 ± 1.3	0.057
Zn	12	3.93 ± 0.04	0.020 ± 0.005		
S	12	4.46 ± 0.05	0.017 ± 0.008		
$CuInS_2$, *k*-range: 2.5–13.					
S	4	2.47 ± 0.01	0.003 ± 0.001	5.5 ± 1.0	0.029
Cu	4	3.85 ± 0.05	0.008 ± 0.007		
In	4	4.02 ± 0.07	0.005 ± 0.011		
Cu	4	4.04 ± 0.06	0.002 ± 0.008		
S	4	4.57 ± 0.06	0.018 ± 0.010		
Sample 501, *k*-range: 2.5–12.					
S	4.21 ± 0.59	2.45 ± 0.01	0.006 ± 0.002	8.8 ± 1.5	0.049
Zn	12	3.92 ± 0.03	0.017 ± 0.004		
S	12	4.48 ± 0.06	0.020 ± 0.011		

(*Continued*)

https://doi.org/10.1180/mgm.2019.10 Published online by Cambridge University Press

Table 3. (*Continued.*)

Scattered atoms	*N*	*r*, Å	σ^2, Å^{-2}	E^0, eV	*R*-factor
Cu *K*-edge[4]					
$CuFeS_2$, *k*-range: 3–12.					
S	4	2.28 ± 0.01	0.006 ± 0.001	5.5 ± 1.4	0.023
Cu	4	3.31 ± 0.10	0.025 ± 0.016		
Fe	4	3.72 ± 0.10	0.024 ± 0.020		
Fe	4	4.17 ± 0.06	0.016 ± 0.009		
$CuInS_2$, *k*-range: 3–12.					
S	4	2.31 ± 0.01	0.009 ± 0.001	4.1 ± 1.3	0.022
In	4	3.22 ± 0.05	0.028 ± 0.008		
In	4	4.11 ± 0.07	0.029 ± 0.023		
Cu	4	4.11 ± 0.07	0.020 ± 0.011		
Sample 501, *k*-range: 3–12.					
S	4.29 ± 1.67	2.30 ± 0.03	0.007 ± 0.005	2.2 ± 4.4	0.038
Au L_3-edge[5]					
Au_2S, synthetic, *k*-range: 3– 13					
S	2	2.30 ± 0.01	0.004 ± 0.001	4.8 ± 0.7	0.015
Au	6	3.68 ± 0.06	0.018 ± 0.007		
MS[6]	12	4.08 ± 0.08	0.007 ± 0.008		
MS[7]	2	4.55 ± 0.02	0.007 ± 0.003		
Sample 1450, *k*-range: 3–12, fitting in *R*-space, *R*-range: 1.2–3.0					
S	2.39 ± 0.27	2.35 ± 0.01	0.008 ± 0.001	0.4 ± 1.3	0.015
Sample 1661, *k*-range: 3–11, fitting in *R*-space, *R*-range: 1.2–3.0					
S	2.48 ± 0.34	2.35 ± 0.01	0.008 ± 0.002	0.7 ± 1.5	0.018
Cd *K*-edge[8]					
CdS, synthetic, *k*-range: 3–11.					
S	4	2.59 ± 0.02	0.014 ± 0.003	1.9 ± 1.7	0.039
Sample 501, *k*-range: 3–13.					
S	3.76 ± 0.53	2.51 ± 0.01	0.004 ± 0.001	15.1 ± 1.5	0.074
Zn	12	3.97 ± 0.06	0.023 ± 0.008		
MS[9]	24	4.03 ± 0.07	0.007 ± 0.007		
S	12	4.54 ± 0.06	0.020 ± 0.010		

[1]$S_0^2 = 0.85$ (ZnS); [2]$S_0^2 = 0.75$ (FeS_2); [3]sphalerite structure from Jamieson and Demarest (1980) was used as initial model for EXAFS fitting, $S_0^2 = 0.95$ was calculated from fitting of In_2S_3 model spectra; [4]$S_0^2 = 0.75$ ($CuInS_2$); [5]Au_2S structure (Ishikawa *et al.*, 1995) was used as initial model for EXAFS fitting, the value of $S_0^2 = 0.84$ calculated from fitting of Au_2S model spectra was used for fitting of Au–In-sphalerite spectra; [6]MS: Au–Au –S–Au; [7]MS: Au–S–Au–S–Au; [8]$S_0^2 = 0.95$ (CdS); [9]MS: Cd–Zn–S–Cd.

Fig. 8 (Cd K-edge). Figures S2 and S3 show Zn and Fe *K*-edge spectra, respectively.

Zinc and iron K-edges

The local atomic structures around Zn and Fe (coordination numbers and interatomic distances) are identical within the uncertainty of the experimental data, and correspond to pure sphalerite (Zn,Fe)S (top of Table 3).

Indium K-edge

The best fit of the experimental spectra of Au–In and Cu–In-bearing sphalerites was achieved when In substitutes for Zn in the sphalerite lattice. Analysis of the experimental spectra yields no difference in the local atomic environment of In regardless of the composition of minerals (Table 3, Fig. 6). In the structure of sphalerite a cation is tetrahedrally coordinated by S atoms; the 2nd coordination shell consists of 12 Zn atoms, and the 3rd coordination shell contains 12 S atoms (Fig. 5). Preliminary fitting of the experimental spectra were performed with calculation of the coordination numbers of atoms in the 2nd and 3rd coordination shells. The calculated values of *N* varied between 10 and 19, but the uncertainty of the single values was quite large. Therefore, during the final fits these values were fixed in accordance with the sphalerite structure parameters ($N = 12$).

Data in Table 3 indicate that the In–S distance increased by 0.12 Å with respect to the crystal structure of pure sphalerite in the 1st coordination shell, by 0.09–0.1 Å for Zn atoms in the 2nd shell, whereas the In–S distance for the 3rd coordination shell is close to that of pure ZnS. Thus, our data demonstrate that the distortion of the sphalerite crystal structure, caused by the replacement of Zn with In, decreases for distant coordination shells and disappears at $R > 4.6$ Å. This observation is consistent with results obtained for semiconducting In- and Ga-bearing materials with tetrahedral coordination polyhedra (Schnohr, 2015). The admixture of Fe (up to 10 wt.%) and Cd (up to 7.5 wt.%) does not change the structural parameters of In.

Regardless of the high Au concentrations, we did not observe a contribution of this heavy atom to In *K*-edge EXAFS spectra up to the 3rd coordination shell. These results imply the possibility of the formation of In-bearing solid solution in sphalerite without the Au–In clustering. Generalising these results to all the group 11 metals we suggest that the charge compensation coupled substitution scheme, $2Zn^{2+} \leftrightarrow (Cu,Ag,Au)^{1+} + In^{3+}$, may take place in sphalerite without formation of roquesite ($CuInS_2$) and, probably for Ag, laforêtite ($AgInS_2$) components in solid solution. This implies that In and the group 11 metals are statistically (randomly) distributed within the sphalerite matrix. The $R_{In-S} = 2.46 \pm 0.01$ Å determined in the present study for the first coordination shell of Au–In- and Cu–In-bearing sphalerites agrees within uncertainty levels with the value determined for synthetic Cu–In-bearing phases in Pattrick *et al.* (1998) and Fieber-Erdmann *et al.* (1999), as well as with the R_{In-S} in roquesite.

Gold L_3-edge

The nearest neighbours of Au in sphalerite are S atoms with $N_S \approx 2.5$. The Au–S distance of 2.35 Å is higher than in Au_2S where Au is linearly coordinated with S atoms ($N_S = 2$, $R_{Au-S} = 2.30$ Å, Table 3 and Fig. 7*a*). In contrast to In, for which the structural parameters can be obtained up to the 3rd coordination shell with 12 S atoms, the absence of a distinct maximum of the Fourier transform for Au L_3-edge EXAFS spectra at $R > 2.5$ Å implies that the second coordination shell of Au is of a disordered nature. The mentioned values of *N* and *R*, the complex line shape of HERFD-XANES spectra with broad asymmetric white lines (Fig. 4), as well as disordered distant coordination shells, might be interpreted as the presence of at least two different forms of Au. Comparing these data with results reported in the literature for Cu-bearing (In-free) sphalerites (Warkentin *et al.*, 2007) and taking into account the similarity of Cu and Au chemical properties, we suggest that these forms can be Au_2S clusters ($R_{Au-S} \sim 2.3$ Å) and a small admixture of the Au solid solution with higher Au–S distance ($R_{Au-S} \sim 2.5$ Å in accord with DFT calculations, see section 'DFT calculations and atomic charges'). We note here that the crystal structures of CuS and Au_2S are different, but at the nanoscale level both geometric and electronic factors are important in stabilisation of the (nano)clusters (c.f., Tofanelli and Ackerson, 2012). The pronounced increase by ~0.2 Å of the Au–S distance in Au solid solution with respect to the Zn–S distance in pure sphalerite can be explained by a large difference in the ionic radii of these metals (0.6 Å for Zn vs 1.37 Å for Au, Shannon, 1976). Apart from chemical analogy with Cu, the following facts argue for the presence of Au_2S clusters: (1) the coordination number N_s is close to 2; (2) the interatomic distance R_{Au-S} is close to 2.3 Å; and (3) the size of the Au-bearing inclusions is submicroscopic (Fig. 2*a*). Our data, however, do not allow us to determine whether the Au_2S clusters were formed at the synthesis temperature, or formed as a quench product of the solid solution breakdown. Similarly to CuS in

https://doi.org/10.1180/mgm.2019.10 Published online by Cambridge University Press

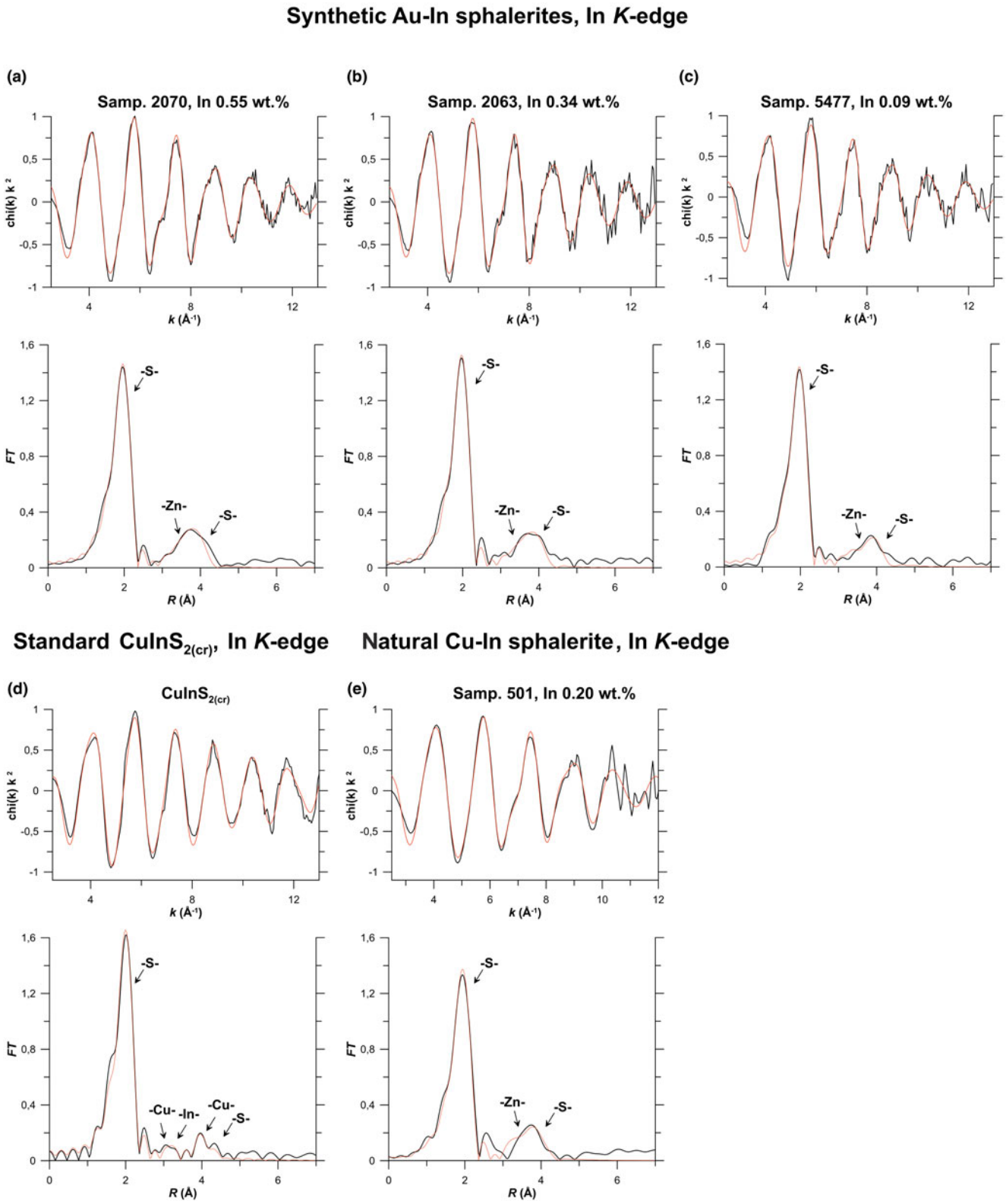

Fig. 6. Results of In *K*-edge EXAFS spectra fitting. Synthetic Au–In sphalerites, Samples: (*a*) 2070; (*b*) 2063; and (*c*) 5477. Natural Cu–In sphalerite: (*d*) Sample 501; and (*e*) standard – roquesite $CuInS_{2(cr)}$. *Top*: k^2-weighted background-subtracted EXAFS spectra, *Bottom*: Fourier transforms (FT) of the k^2-weighted EXAFS spectra (not corrected for phase shift). Black lines – experiment, red lines – fit results. Scattering atoms are indicated near FT peaks, MS – multiple-scattering contributions. Results of the fitting are listed in Table 3.

https://doi.org/10.1180/mgm.2019.10 Published online by Cambridge University Press

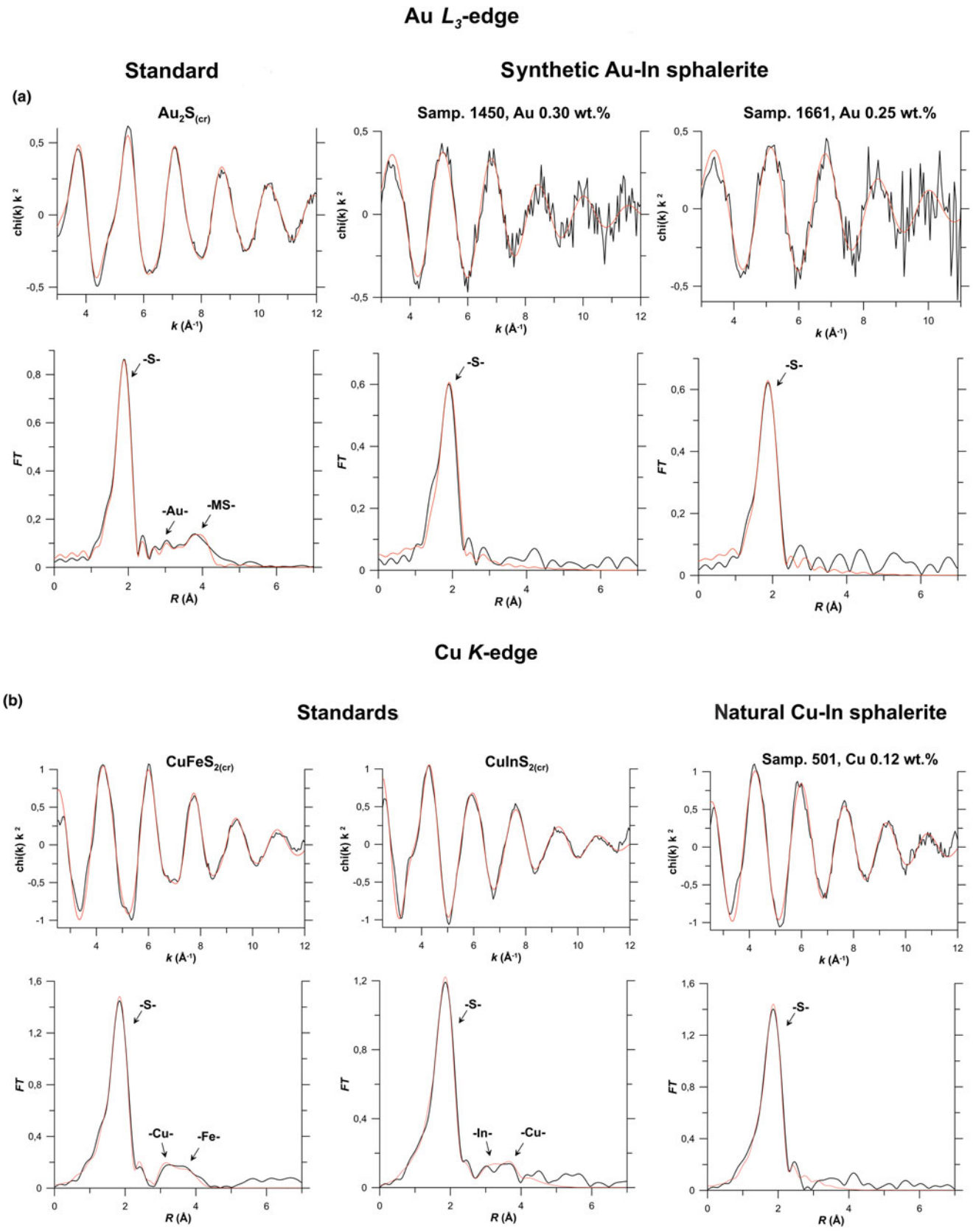

Fig. 7. Results of Au L_3-edge and Cu *K*-edge EXAFS spectra fitting. (*a*) Au L_3-edge: synthetic Au–In sphalerites for Samples 1450, 1661 and standard $Au_2S_{(cr)}$. (*b*) Cu *K*-edge: natural Cu–In sphalerite (Sample 501), and standards chalcopyrite $CuFeS_{2(cr)}$ and roquesite $CuInS_{2(cr)}$. For the legend see caption to Fig. 6, MS – multiple-scattering contributions.

https://doi.org/10.1180/mgm.2019.10 Published online by Cambridge University Press

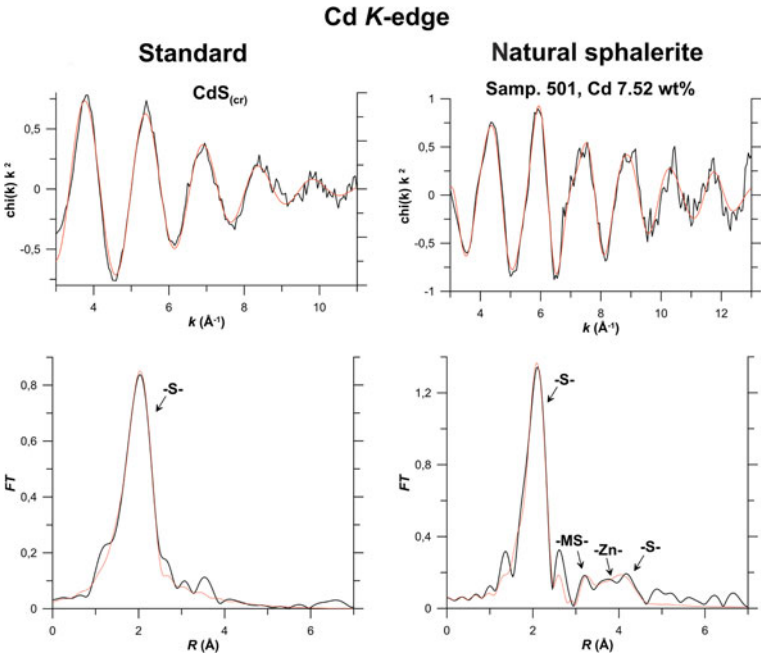

Fig. 8. Results of Cd *K*-edge EXAFS spectra fitting of natural sphalerite (Sample 501), and standard synthetic $CdS_{(cr)}$. For the legend see caption to Fig. 6; MS – multiple-scattering contributions.

Cu-bearing sphalerite (Warkentin *et al.*, 2007), the Au_2S clusters can be integrated into the sphalerite host matrix in accordance with the crystallographic axes of the sphalerite structure, which can stabilise the metastable gold sulfide.

The absence of a contribution from the In atom in the distant coordination shells of Au is an additional argument for the absence of the Au–In clustering. We can speculate that at high temperatures Au existed mostly in the solid-solution state, decomposing upon cooling into Au_2S clusters. Evidence might be (1) the concentration of Au in sphalerite is proportional to the In content (these elements can form an isomorphous solid solution via the charge compensation scheme), and (2) Au_2S is a metastable phase which decomposes at high temperatures (Tagirov *et al.*, 2006). However, the characterisation of Au in sphalerite at high temperatures can only be determined unambiguously by *in situ* spectroscopic experiments on sphalerite being heated to the formation (synthesis) temperature.

Copper K-edge

In contrast to Au, the Cu *K*-edge EXAFS spectrum is best described by the solid-solution model with $N_S \approx 4$ (Table 3). The Fourier transform of EXAFS spectra in the region of distant coordination shells ($R > 3$ in Fig. 7*b*) is different from those of reference substances – $CuFeS_2$ and $CuInS_2$. The distant coordination shells of Cu in Cu–In-bearing sphalerite are disordered in contrast to the reference substances. This is the common feature of Cu–In- and Au–In-bearing sphalerites. The distance to the S atoms in the 1st coordination shell is 2.30 Å which is shorter by 0.04 Å than the Zn–S distance in pure sphalerite.

Cadmium K-edge

As indicated by data presented in Fig. 8 and Table 3, the best fit of the Cd *K*-edge EXAFS spectrum is attained for the solid-solution model. The contributions of the distinct atomic groups are clearly distinguishable up to the 3rd coordination shell of Cd. As in the case of In, the 1st coordination shell of the cation exhibits considerable expansion of 0.17 Å compared to the pure sphalerite structure, the 2nd coordination shell expands by 0.14 Å, whereas the expansion of the 3rd shell is much less pronounced: the *Me*–S distances of Cd-bearing and pure sphalerite are identical within the experimental uncertainty. No Cd–Cd clustering is observed which means that Cd is randomly distributed within the sphalerite matrix. Note that the absence of the contributions from the distant coordination shells in the spectrum of $CdS_{(cr)}$ can be related to the low quality of the material which was obtained by means of reaction of aqueous Cd acetate solution with hydrogen sulfide in a hydrothermal reactor, and has not been subjected to ageing.

DFT calculations and atomic charges

Results of relaxation of atomic structures performed using the DFT method are given in Table 4. As can be seen in the last two columns of Table 4, an excellent agreement (within 0.02–0.03 Å) is observed between the simulated structure of pure sphalerite ZnS and interatomic distances calculated from the XRD data, as well as with results of the EXAFS spectra fitting (Table 3). These data demonstrate the high accuracy of the DFT method in modelling of sphalerite-type structures. For In the EXAFS model (Table 3) was adequately reproduced by DFT simulation for the solid solution formed via the scheme $2Zn \leftrightarrow (In + Au)$ with In and Au atoms located far from each other (without Au–In clustering). In this case the difference between DFT calculation and EXAFS spectra fitting is 0.02, 0.01 and 0.04 Å for the 1st, 2nd, and 3rd coordination shells, respectively. For the case when In and Au are placed in the adjacent cationic positions there is considerable splitting of interatomic distances in the 1st and 2nd coordination shells of In and Au. This splitting would result in unrealistically high values of Debye–Waller parameters which were not observed in the EXAFS model. The same scheme can be applied to Cu–In-bearing sphalerites although the splitting is less pronounced (0.05 Å for in the 1st coordination shell of In

https://doi.org/10.1180/mgm.2019.10 Published online by Cambridge University Press

Table 4. Interatomic distances in sphalerite with and without In, Au and Cu dopants determined by DFT calculations. Literature data on interatomic distances for the unrelaxed pure sphalerite structure are given at the bottom of the table.

		Coordination shells							
		Me–S		*Me*–Zn		*Me*1–*Me*2		*Me*–S	
Bond		*N*	*R*, Å	*N*	*R*, Å	*N*	*R*, Å	*N*	*R*, Å
ZnS+Au	*Me* = Au	4	2.48	12	3.87	–	–	12	4.52
ZnS+Cd	*Me* = Cd	4	2.52	12	3.90	–	–	12	4.52
ZnS+In	*Me* = In	4	2.50	12	3.93	–	–	12	4.53
ZnS+Au+In (In and Au atoms are located in neighbouring sites)	*Me*1=In	4	2.43, 2.49, 2.49, 2.50	12	3.90–3.95	1	3.92	12	4.52–4.54
	*Me*2=Au	4	2.48, 2.47, 2.47, 2.55	12	3.87–4.00			12	4.51–4.59
ZnS+Au+In (In and Au atoms are located far from each other)	*Me*1=In	4	2.48	12	3.93	1	12.78	12	4.52
	*Me*2=Au	4	2.50	12	3.86			12	4.52
ZnS+Cu+In (In and Cu atoms are located in neighbouring sites)	*Me*1=In	4	2.46, 2.50, 2.50, 2.51	12	3.85–3.97	1	3.87	12	4.50–4.54
	*Me*2=Cu	4	2.31, 2.32, 2.32, 2.34	12	3.82–3.92			12	4.45–4.55
ZnS+Cu+In (In and Cu atoms are located far from each other)	*Me*1=In	4	2.49	12	3.93	1	12.78	12	4.53
	*Me*2=Cu	4	2.33	12	3.81			12	4.51
ZnS		4	2.36	12	3.86	–	–	12	4.51
ZnS, literature XRD data, Jamieson and Demarest (1980)		4	2.34	12	3.83	–	–	12	4.49

in Cu–In-bearing sphalerite vs. 0.07 Å for the In–Au-bearing one, Table 4). This splitting is still significant for the value of Debye–Waller parameter.

Another possibility to obtain the charge compensation is the scheme $3Zn^{2+} \leftrightarrow 2In^{3+} + \square$, where $\square$ is the cationic sublattice vacancy. The second part of Table 4 indicates that results of DFT calculations for this compensation scheme, when two In atoms and a vacancy are located far from each other, are close to the EXAFS data (Table 3). This scheme, however, cannot explain the direct correlation between In and Au contents and, therefore, can be rejected.

In the case of Au, the agreement between the DFT simulation and EXAFS fit is poor. This means that the most of Au is not in the solid-solution state, but, as has been shown by the EXAFS spectra fitting, presents in the form of Au_2S clusters. The minor contribution of the solid-solution Au is reflected in the increase of the Au–S distance in the 1st coordination shell of Au determined by the EXAFS spectra fitting, and increase of the number of the sulfur atoms nearest to Au (in the solid-solution state $R_{Au-S} = 2.5$ Å and $N_S = 4$, Table 4).

The agreement between the DFT simulation and EXAFS spectra fitting of Cd-bearing sphalerite is fairly good (within 0.01 Å for the 1st coordination shell and 0.02 Å for the 3rd one). For the 2nd coordination shell the calculated distance differs from the EXAFS model by 0.07 Å which is close to the EXAFS fit uncertainty of 0.06 Å. This calculation confirms the solid-solution state of Cd.

The results of the Bader analysis of electron density performed using QTAIM are summarised in Table S1. The partial atomic charge of In in sphalerite is more positive than that of In in InS and In_2S_3 (+1.2 ± 1.3 *e* for In-bearing sphalerites vs. +0.7 ± 0.8 *e* for In sulfides). The more positive charge is consistent with analysis of In *K*-edge XANES spectra and reflects the more efficient transfer of the negative charge from In to ligands (S) in the solid-solution state. The positive charge of Au slightly decreases when it is incorporated into the sphalerite structure in comparison with Au_2S, whereas the charge of Cu in sphalerite is much more positive compared to the charge of Au (+0.52 *e* for Cu *vs.* +0.17 *e* for Au). This is explained by the fact that Au is the most electronegative metal (χ(Au) = 2.54) whose electron affinity is higher than that of Zn, In and Cu. It is interesting to note that the charges of In, Au and Cu are almost independent to the mechanism of their incorporation into the structure of sphalerite. This means that in sphalerite the redistribution of delocalised electrons due to isomorphic substitutions takes place not only between the nearest atoms, but involves remote atoms located far from the admixture within the bulk sphalerite structure, which is consistent with the absence of Cu–In and Au–In clustering.

Concentration and state of admixtures in sphalerite

In general, one can say that sphalerite can host high (up to economic) concentrations of admixtures of many critical and strategic elements in the solid-solution state. All admixtures, which were determined at trace/minor level in sphalerite samples studied in the present work (Cd, Mn, In, Cu, Au and Se), are distributed homogeneously within the host mineral matrix. The concentration of critical elements (Cd, In, Au and Se) in sphalerite, formed at high temperature, can reach a level of a few tenth of wt.% (a few wt.% for Cd). These data imply that the concentration of the admixtures in the solid-solution state increases with increasing temperature. At the ore formation temperature the solubility of dopants, apart from the temperature, is governed by the difference in the ionic radii with the main component (Zn). The concentration of heterovalent dopants in sphalerite also depends on the concentration of the adjacent admixture (In in the case of Cu and Au).

Results of the present study demonstrate that at low concentrations (<1 wt.%) inherent to natural sphalerites, In is in the solid-solution state independently of the adjacent metal type (Cu or Au). There are some indications that the formation of the sphalerite solid solution can take place without In–In, Au–Au, Au–In and Cu–In clustering, which means that all these elements are distributed randomly in the sphalerite matrix. These indications are: (1) the differences in the Cu *K*-edge XANES spectra of Cu–In-bearing natural sphalerite and $CuInS_2$; (2) an absence of the heavy-atom contributions to the EXAFS signal corresponding to the 2nd coordination shell of In and Cu (Au in the case of In *K*-edge spectra, and In in the case of Cu *K*-edge one); and (3) according to DFT simulations, Cu–In clustering would produce a notable splitting of interatomic distances which was not observed in the results of Cu and In *K*-edge EXAFS spectra fitting. We note, however, that these

https://doi.org/10.1180/mgm.2019.10 Published online by Cambridge University Press

indications are indirect, and the problem of clustering in the sphalerite solid solution needs further examination.

Similarly In, with an ionic radius of 0.62 Å (Shannon, 1976) is close to Zn (0.6 Å), Cu (ionic radius 0.6 Å) withstands cooling and at ambient temperature exists in the solid-solution state. Direct correlation between the concentrations of Au and In in the synthesised sphalerite crystals imply that Au is also present in the solid-solution state at the synthesis parameters up to Au concentrations of a few tenth of wt.%. The Au solid solution, however, decomposes during cooling with the formation of Au_2S clusters because of the large ionic radius of Au (1.37 Å, octahedral coordination, there is no data for tetrahedral geometry). The presence of the second, minor form of Au, which is detected in sphalerite together with the Au_2S clusters and can be assigned to the solid solution, is indicated by: (1) the number of the nearest to Au S atoms $N_S > 2$, whereas $N_S = 2$ in Au_2S; (2) the Au–S distance in the 1st coordination shell $R_{Au-S} = 2.35$ Å, which is higher than the $R_{Au-S} = 2.30$ Å in Au_2S; and (3) the complex shape of the white line of Au L_3-edge XANES spectra. The ratio of Au solid solution to Au_2S clusters, calculated using the average value of $R_{Au-S} \sim 2.35$ Å, obtained by means of the EXAFS spectra fitting, equals 0.05. This calculation implies that at ambient temperature Au in Au–In-bearing sphalerites exists in the solid-solution state at concentrations up to a few tens of ppm. Therefore, Au in natural Cu–In-bearing sphalerite sampled at Kudriavy volcano can be expected to be in the solid-solution state (the Au concentration is 7 ppm).

Our results demonstrate that all metals of group 11 of the periodic system (*Me* = Cu, Ag and Au) can form an isomorphous solid solution in sphalerite via the charge compensation scheme $2Zn^{2+} \leftrightarrow Me^{+} + Me^{3+}$, where Me^{3+} is a metal in +3 oxidation state. Apart from In^{3+} it can be a cation of another chalcophile element, for example, Tl^{3+}, As^{3+}, Sb^{3+}, Bi^{3+}, or Fe^{3+}. The most probable candidate for this substitution is As^{3+} with ionic radius close to the radius of Zn^{2+} (0.58 Å (As) vs. 0.6 Å (Zn)). Because ionic radii of the other elements listed above in +3 oxidation state differ significantly from the radius of Zn^{2+} (0.76 Å (Sb), 0.75 Å (Tl), and 0.49 Å (Fe)) the solid solutions, formed at high temperature, will be of narrower composition range compared to In. The solid solutions involving these elements either decompose upon cooling, or represent a metastable phase which has not undergone a breakdown due to slow kinetics. The state of Ag in sphalerite, however, has to be determined by EXAFS spectroscopic experiments preformed on Ag- and Ag–In-bearing minerals. This is an ongoing study in our laboratory.

Formation of the solid solution $2Zn^{2+} \leftrightarrow Au^{+} + Fe^{3+}$ is confirmed by high concentrations of Au (0.02 wt.% Au) in In-free Fe-bearing sphalerite, Sample 1440. The shape of Au L_3 HERFD-XANES spectra of this sample is similar to the spectra of Au–In sphalerite which implies similar speciation of Au, but the Au concentration is ~10 times lower because of the lower concentration of Fe^{3+} compared to In^{3+}. The reason for the low Fe^{3+} concentration is considerable difference in ionic radii of Fe^{3+} and Zn^{2+}. The concentration of Fe^{3+} in Sample 1440 can be estimated as ~0.005 wt.% from the suggested substitution mechanism. However, during cooling and decomposition of the solid solution with the formation of Au_2S clusters, the Fe^{3+} also may change its oxidation state to Fe^{2+}. The true oxidation state of Fe in sphalerites at ambient temperature can be revealed only by means of Mössbauer spectroscopy.

Conclusions

For the present study we synthesised crystals of In and Au-bearing sphalerite (Zn,Fe)S with dopants in concentrations of 0.03–0.5 wt.%. Results of EPMA and LA-ICP-MS chemical analyses showed that both In and Au are distributed homogeneously within the sphalerite matrix. X-ray absorption spectroscopy was applied in order to determine the local atomic environment and the valence state of In and Au in the synthesised crystal samples, which were compared to the natural Cu–In-bearing sphalerite sampled at the Kudriavy volcano (Iturup Island, Russia). In accordance with XANES spectroscopy these elements are present in sphalerite in +3 (In) and +1 (Au, Cu) formal oxidation states. At ambient temperature In exists in sphalerite in the solid-solution state where it replaces Zn. Analysis of EXAFS spectra shows that the bond lengths of In increase (with respect to pure ZnS) from 2.34 to 2.46 Å in the 1st coordination shell (where In is tetrahedrally coordinated by S), from 3.83 to 3.92 Å in the 2nd coordination shell ($N_{Zn} = 12$), and is close to the *Me*–S distance of the pure sphalerite for the 3rd coordination shell ($N_S = 12$, $R_{In-S} = 4.46$–4.48 Å). Gold, in contrast to In, mainly exists in the form identified as Au_2S clusters with average $R_{Au-S} \approx 2.3$ Å, and a small portion of the second form with $R_{Au-S} \approx 2.5$ Å which is attributed to the Au solid solution. The second coordination shell of Au is of disordered nature. The Au_2S clusters, most probably, are the quench product of high temperature Au–In-bearing solid solution which was stable at the synthesis temperature. Copper in natural sphalerite is in the solid-solution state. The Cu–S distance in the 1st coordination shell is equal to 2.30 Å which is 0.04 Å lower than the Zn–S distance in pure sphalerite, whereas the distant coordination shells, like Au–In sphalerites, are of disordered character. Cadmium is distributed randomly within the natural sphalerite matrix and exists in the solid-solution state. The 1st coordination shell of Cd expands by 0.17 Å compared to the pure sphalerite structure, the 2nd coordination shell expands by 0.14 Å, whereas the Cd–S distance in the 3rd coordination shell is close to the Zn–S distance of pure sphalerite. These data demonstrate that the homogeneous character of a trace-element distribution, which is often observed in natural sulfide minerals, doesn't confirm formation of the solid solution, but can be explained by the presence of clusters or nano-sized particles disseminated in the host mineral matrix such as Au_2S clusters. These clusters/particles can be formed because of the breakdown of the solid solution that was stable at the ore formation conditions. The final state of trace elements, which corresponds to ambient conditions, depends on the difference of the ionic radii between the trace element and the main component of the sulfide mineral (Zn in sphalerite in the present case), the presence of the conjugated charge-compensating element (In, Fe), and the trace-element concentration. When the ionic radii of trace and main components are close to each other, and the concentration of trace element is low enough, the metastable solid solution can withstand cooling like Cu–In-bearing sphalerites. If the difference in the ionic radii is considerable and trace elements are present in relatively elevated concentrations, most of the solid solution decomposes, and only a small portion of the trace element is present in the solid-solution state, as has been observed in the Au–In-bearing sphalerites. In natural sphalerites the concentration of Au and Ag (the other group 11 metal) rarely exceed a few tens of ppm and they coexist with Fe^{3+}, In^{3+}, or other metals in +3 oxidation state. Therefore, one can suggest that in natural sphalerites both Au and Ag are mostly present in the solid-solution state formed by the charge compensation scheme $2Zn^{2+} \leftrightarrow Me^{+} + Me^{3+}$.

Acknowledgements. The authors thank the ESRF scientific council for the beamtime allocation under proposal Nos 20-01-782, ES-703 (ROBL) and

https://doi.org/10.1180/mgm.2019.10 Published online by Cambridge University Press

ES-184 (ID26), and STM beamline team (KSRS) for technical support during the experiment. The help and support of Joerg Exner (ROBL) is greatly appreciated. We are grateful to Vera Abramova and Elena Minervina for chemical analyses of synthesised minerals using LA-ICP-MS methods. We would like to acknowledge the three anonymous reviewers and the Associate Editor for important comments that improved the quality of the manuscript. This study was supported by the Russian Science Foundation grant No. 14-17-00693-П (XAS experiments with Au–In sphalerites), Russian Science Foundation grant No. 18-77-00078 (XAS experiments with Cu–In sphalerite and DFT calculations), and Russian Foundation for Basic Research grant No. 16-05-00938 (crystal growth experiments). Quantum chemical calculations have been carried out using computing resources of the Federal collective usage centre Complex for Simulation and Data Processing for Mega-science Facilities at NRC "Kurchatov Institute" (ministry subvention under agreement RFMEFI62117X0016), http://ckp.nrcki.ru/. Chemical analyses were performed at the "IGEM-Analytica" Center for Collective Use.

Supplementary material. To view supplementary material for this article, please visit https://doi.org/10.1180/mgm.2019.10

References

Apple E.F. and Williams F.E. (1959) Associated donor-acceptor luminescent centers in zinc sulfide phosphors. *Journal of the Electrochemical Society*, **106**, 224–230.

Bader R.F.W. (1990) *Atoms in Molecules: a Quantum Theory*. Oxford University Press, Oxford, U.K.

Bader R.F.W. (1991) A quantum theory of molecular structure and its applications. *Chemical Reviews*, **91**, 893–928.

Belissont R., Muñoz M., Boiron M.-C., Luais B. and Mathon O. (2016) Distribution and oxidation state of Ge, Cu and Fe in sphalerite by μ-XRF and *K*-edge μ-XANES: insights into Ge incorporation, partitioning and isotopic fractionation. *Geochimica et Cosmochimica Acta*, **177**, 298–314.

Blöhl P.E. (1992) Projector augmented-wave method. *Physical Review B*, **50**, 17953–17979.

Bonnet J., Cauzid J., Testemale D., Kieffer I., Proux O., Lecomte A. and Bailly L. (2017) Characterization of germanium speciation in sphalerite (ZnS) from Central and Eastern Tennessee, USA, by X-ray absorption spectroscopy. *Minerals*, **7**, 79.

Bortnikov N.S., Cabri L.J., Vikentiev I.V., Tagirov B.R., Mc Mahon G., Bogdanov Yu.A. and Stavrova O.O. (2003) Invisible gold in sulfides from seafloor massive sulfide edifices. *Geology of Ore Deposits*, **45**, 201–212.

Burke E.A.J. and Kieft C. (1980) Roquesite and Cu–In-bearing sphalerite from Långban, Bergslagen, Sweden. *The Canadian Mineralogist*, **18**, 361–363.

Chaplygin I.V., Mozgova N.N., Mokhov A.V., Koporulina E.V., Bernardt H.-J. and Bryzgalov I.A. (2007) Minerals of the system ZnS-CdS from fumaroles of the Kudriavy volcano, Iturup island, Kuriles, Russia. *The Canadian Mineralogist*, **45**, 709–722.

Chareev D.A. (2016) General principles of the synthesis of chalcogenides and pnictides in salt melts using a steady-state temperature gradient. *Crystallography Reports*, **61**, 506–511.

Chareev D.A., Volkova O.S., Geringer N.V., Koshelev A.V., Nekrasov A.N., Osadchii V.O., Osadchii E.G. and Filimonova O.N. (2016) Synthesis of chalcogenide and pnictide crystals in salt melts using a steady-state temperature gradient. *Crystallography Reports, 61*, 682–691.

Chareev D.A., Osadchii V.O., Shiryaev A.A., Nekrasov A.N., Koshelev A.V. and Osadchii E.G. (2017) Single-crystal Fe-bearing sphalerite: synthesis, lattice parameter, thermal expansion coefficient and microhardness. *Physics and Chemistry of Minerals*, **44**, 287–296.

Chernyshov A.A., Veligzhanin A.A. and Zubavichus Y.V. (2009) Structural materials science end-station at the Kurchatov Synchrotron Radiation Source: Recent instrumentation upgrades and experimental results. *Nuclear Instruments and Methods in Physics Research A*, **603**, 95–98.

Cook N.J., Ciobanu C.L., Pring A., Skinner W., Shimizu M., Danyushevsky L. and Melcher F. (2009) Trace and minor elements in sphalerite: A LA-ICPMS study. *Geochimica et Cosmochimica Acta*, **73**, 4761–4791.

Cook N.J., Ciobanu C.L., Brugger J., Etschmann B., Howard D.L., de Jonge M.D., Ryan C. and Paterson D. (2012) Determination of the oxidation state of Cu in substituted Cu–In-Fe-bearing sphalerite via m-XANES spectroscopy. *American Mineralogist*, **97**, 476–479.

Cook N.J., Etschmann B., Ciobanu C.L., Geraki K., Howard D.L., Williams T., Rae N., Pring A., Chen G., Johannessen B. and Brugger J. (2015) Distribution and substitution mechanism of Ge in a Ge-(Fe)-bearing sphalerite. *Minerals*, **5**, 117–132.

Corrado C., Jiang Yu., Oba F., Kozina M., Bridges F. and Zhang J.Z. (2009) Synthesis, structural, and optical properties of stable ZnS:Cu,Cl nanocrystals. *Journal of Physical Chemistry A*, **113**, 3830–3839.

Fieber-Erdmann M., Rossner H., Holub-Krappe E., Eyert V. and Luck I. (1999) Structural properties of $Zn_{2-2x}(CuIn)_xS_2$ ($X \leq 1$) solid solution thin film obtained by EXAFS. *Journal of Synchrotron Radiation*, **6**, 474–476.

Fletcher R. (1987) *Practical Methods of Optimization* (2nd ed.). John Wiley & Sons, New York.

Galoisy L. (2004) X-ray absorption spectroscopy in geosciences: Information from the EXAFS region. Pp. 553–587 in: *Spectroscopic Methods in Mineralogy* (A. Beran and E. Libowitzky, editors). EMU Notes in Mineralogy, **Vol. 6**.

Gauthier C., Sole V.A., Signorato R., Goulon J. and Moguiline E. (1999) The ESRF beamline ID26: X-ray absorption on ultra dilute sample. *Journal of Synchrotron Radiation*, **6**, 164–166.

Giannozzi P., Baroni S., Bonini N., Calandra M., Car R., Cavazzoni C., Ceresoli D., Chiarotti G.L., Cococcioni M., Dabo I., Corso A.D., de Gironcoli S., Fabris S., Fratesi G., Gebauer R., Gerstmann U., Gougoussis C., Kokalj A., Lazzeri M., Martin-Samos L., Marzari N., Mauri F., Mazzarello R., Paolini S., Pasquarello A., Paulatto L., Sbraccia C., Scandolo S., Sclauzero G., Seitsonen A.P., Smogunov A., Umari P. and Wentzcovitch R.M. (2009) QUANTUM ESPRESSO: a modular and open-source software project for quantum simulations of materials. *Journal of Physics: Condensed Matter*, **21**, 395502.

Glatzel P. and Bergman U. (2005) High resolution 1s core hole X-ray spectroscopy in 3d transition metal complexes - electronic and structural information. *Coordination Chemistry Reviews*, **249**, 65–95.

Glatzel P., Weng T.-C., Kvashnina K., Swarbrick J., Sikora M., Gallo E., Smolentsev N. and Mori R.A. (2013) Reflections on hard X-ray photon-in/photon-out spectroscopy for electronic structure studies. *Journal of Electron Spectroscopy and Related Phenomena*, **188**, 17–25.

Herzig P.M., Hannington M.D., Fouquet Y., von Stackelberg U. and Petersen S. (1993) Gold-rich polymetallic sulfides from the Lau back arc and implications for the geochemistry of gold in sea-floor hydrothermal systems of the Southwest Pacific. *Economic Geology*, **88**, 2182–2209.

Ishikawa K., Isonga T., Wakita S. and Suzuki Y. (1995) Structure and electrical properties of Au_2S. *Solid State Ionics*, **79**, 60–66.

Iwanowski R.J. and Ławniczak-Jabłońska K. (1996) EXAFS studies of local atomic structure in $Zn_{1-x}Mn_xS$. *Solid State Communications*, **97**, 879–885.

Iwanowski R.J. and Ławniczak-Jabłońska K. (1997) EXAFS determination of bond lengths in $Zn_{1-x}Fe_xS$ ternary alloys. *Acta Physica Polonica A*, **91**, 797–801.

Iwanowski R.J., Ławniczak-Jabłońska K., Gołacki Z. and Traverse A. (1998) Tetrahedral covalent radii of Mn, Fe, Co and Ni estimated from extended X-ray absorption fine structure studies. *Chemical Physics Letters*, **283**, 313–318.

Jamieson J.C. and Demarest Jr. H.H. (1980) A note on the compression of cubic ZnS. *Journal of Physics and Chemistry of Solids*, **41**, 963–964.

Johan Z. (1988) Indium and germanium in the structure of sphalerite: an example of coupled substitution with copper. *Mineralogy and Petrology*, **39**, 211–229.

Koelmans H. (1960) Association and dissociation of centres in luminescent ZnS-In. *Journal of Physics and Chemistry of Solids*, **17**, 69–79.

Kresse G. (1999) From ultrasoft pseudopotentials to the projector augmented-wave method. *Physical Review B*, **59**, 1758–1775.

Kvashnina K.O. and Scheinost A.C. (2016) A Johann-type X-ray emission spectrometer at the Rossendirf Beamline. *Journal of Synchrotron Radiation*, **23**, 836–841.

Ławniczak-Jabłońska K. and Gołacki Z. (1994) Extended X-ray absorption fine structure studies of Co doped ZnS and ZnSe alloys. *Acta Physica Polonica A*, **86**, 727–735.

Ławniczak-Jabłońska K., Iwanowski R.J., Gołacki Z., Traverse A., Pizzini S. and Fontaine A. (1995) Correlation between XANES of the transition metals in ZnS and ZnSe and their limit of solubility. *Physica B*, **208–209**, 497–499.

Ławniczak-Jabłońska K., Iwanowski R.J., Gołacki Z., Traverse A., Pizzini S., Fontaine A. and Winter I. (1996) Local electronic structure of ZnS and ZnSe doped by Mn, Fe, Co, and Ni from X-ray-absorption near-edge structure studies. *Physical Review B*, **53**, 1119–1128.

Melekestseva I.Yu., Maslennikov V.V., Tret'yakov G.A., Nimis P., Beltenev V.E., Rozhdestvenskaya I.I., Maslennikova S.P., Belogub E.V., Danyushevsky L., Large R., Yuminov A.M. and Sadykov S.A. (2017) Gold- and silver-rich massive sulfides from the Semenov-2 hydrothermal field, 13°31.13′N, Mid-Atlantic Ridge: a case of magmatic contribution? *Economic Geology*, **112**, 741–773.

Mercer C.N. (2015) *Indium: Bringing Liquid-Crystal Displays into Focus*. USGS Report, Fact Sheet 2015–3012, Reston, Virginia, USA.

Mercier-Langevin P., Hannington M.D., Dubé B. and Bécu V. (2011) The gold content of volcanogenic massive sulfide deposits. *Mineralium Deposita*, **46**, 509–539.

Mottana A. (2004) X-ray absorption spectroscopy in mineralogy: Theory and experiment in the XANES region. Pp. 465–552 in: *Spectroscopic Methods in Mineralogy* (A. Beran and E. Libowitzky, editors). EMU Notes in Mineralogy, **Vol. 6**.

Norris D.J., Efros A.L. and Erwin S.C. (2008) Doped nanocrystals. *Nature*, **319**, 1776–1779.

Otero-de-la-Roza A., Blanco M.A., Martín Pendás A. and Luaña V. (2009) Critic: a new program for the topological analysis of solid-state electron densities. *Computer Physics Comunications*, **180**, 157–166.

Otero-de-la-Roza A., Johnson E.R. and Luaña V. (2014) Critic2: A program for real-space analysis of quantum chemical interactions in solids. *Physics Comunications* **185**, 1007–1018.

Pattrick R.A.D, Mosselmans J.F.W. and Charnock J.M. (1998) An X-ray absorption study of doped sphalerites. *European Journal of Mineralogy*, **10**, 239–249.

Ravel B. and Newville M. (2005) ATHENA, ARTEMIS, HEPHAESTUS: data analysis for X-ray absorption spectroscopy using IFEFFIT. *Journal of Synchrotron Radiation*, **12**, 537–541.

Schnohr C.S. (2015) Compound semiconductor alloys: From atomic-scale structure to bandgap bowing. *Applied Physics Reviews*, **2**, 031304.

Schorr S. and Wagner G. (2005) Structure and phase relations of the $Zn_{2x}(CuIn)_{1-x}S_2$ solid solution series. *Journal of Alloys and Compounds*, **396**, 202–207.

Schorr S., Tovar M., Stuesser N., Sheptyakov D. and Geandier G. (2006) Where the atoms are: Cation disorder and anion displacement in $D^{II}X^{VI}$–$A^{I}B^{III}X_2^{VI}$ semiconductors. *Physica B*, **385–386**, 571–573.

Schwarz-Schampera U. (2014) Indium. Pp. 204–229 in: *Critical Metals Handbook* (G. Gunn, editor). Wiley, UK.

Self P.G., Norrish K. and Milnes A.R. (1990) Holes in the background in XRS. *X-Ray Spectrometry*, **19**, 59–61.

Shannon R.D. (1976) Revised effective ionic radii and systematic studies of interatomic distances in halides and chalcogenides. *Acta Crystallographica A*, **32**, 751–767.

Tagirov B.R., Baranova N.N., Zotov A.V., Schott J. and Bannykh L.N. (2006) Experimental determination of the stabilities of $Au_2S_{(cr)}$ at 25°C and Au $(HS)_2^-$ at 25–250°C. *Geochimica et Cosmochimica Acta*, **70**, 3689–3701.

Tagirov B.R., Trigub A.L., Kvashnina K.O., Shiryaev A.A., Chareev D.A., Nickolsky M.S., Abramova V.D. and Kovalchuk E.V. (2016) Covellite CuS as a matrix for "invisible" gold: X-ray spectroscopic study of the chemical state of Cu and Au in synthetic minerals. *Geochimica et Cosmochimica Acta*, **191**, 58–69.

Tofanelli M.A., Ackerson C.J. (2012) Superatom electron configuration predicts thermal stability of $Au_{25}(SR)_{18}$ nanoclusters. *Journal of the American Chemical Society*, **134**, 16937–16940.

Tolcin A.C. (2017) *Indium*. US Geological Survey, Mineral Commodity Summaries, 80–81.

Tonkacheev D.E., Chareev D.A., Abramova V.D., Yudovskaya M.A., Minervina E.A. and Tagirov B.R. (2015) Sphalerite as a matrix for noble, non-ferrous metals and semimetals: A EPMA and LA-ICP-MS study of synthetic crystals. Pp. 847–850 in: *Proceedings of the 13th Biennial SGA Meeting*, 24–27 August 2015, Nancy, France, vol. 2.

Trigub A.L., Tagirov B.R., Kvashnina K.O., Chareev D.A., Nickolsky M.S., Shiryaev A.A., Baranova N.N., Kovalchuk E.V. and Mokhov A.V. (2017) X-ray spectroscopy study of the chemical state of "invisible" Au in synthetic minerals in the Fe-As-S system. *American Mineralogist*, **102**, 1057–1065.

Vikentyev I.V. (2015) Invisible and microscopic gold in pyrite: methods and new data for sulfide ores of the Urals. *Geology of Ore Deposits*, **57**, 237–265.

Vikentyev I.V., Yudovskaya M.A., Mokhov A.V., Kerzin A.L. and Tsepin A.I. (2004) Gold and PGE in massive sulfide ore of the Uzelginsk deposit, Southern Urals, Russia. *The Canadian Mineralogist*, **42**, 651–665.

Warkentin M., Bridges F., Carter S.A. and Anderson M. (2007) Electroluminescence materials ZnS:Cu,Cl and ZnS:Cu,Mn,Cl studied by EXAFS spectroscopy. *Physical Review B*, **75**, 075301.

Wilson S.A., Ridley W.I. and Koenig A.E. (2002) Development of sulfide calibration standards for the laser ablation inductively-coupled plasma mass spectrometry. *Journal of Analytical Atomic Spectrometry*, **17**, 406–409.

Yen W.M. and Weber M.J. (2004) *Inorganic Phosphors: Compositions, Preparation and Optical Properties*. CRC Press, Florida, USA.

Zabinsky S.I., Rehr J.J., Ankudinov A., Albers R.C. and Eller M.J. (1995) Multiple-scattering calculations of X-ray-absorption spectra. *Physical Review B*, **52**, 2995.

https://doi.org/10.1180/mgm.2019.10 Published online by Cambridge University Press